

MIT Joint Program on the Science and Policy of Global Change



Quantifying the Likelihood of Regional Climate Change: A Hybridized Approach

*C. Adam Schlosser, Xiang Gao, Kenneth Strzepek, Andrei Sokolov, Chris E.
Forest, Sirein Awadalla, and William Farmer*

**Report No. 205
October 2011**

The MIT Joint Program on the Science and Policy of Global Change is an organization for research, independent policy analysis, and public education in global environmental change. It seeks to provide leadership in understanding scientific, economic, and ecological aspects of this difficult issue, and combining them into policy assessments that serve the needs of ongoing national and international discussions. To this end, the Program brings together an interdisciplinary group from two established research centers at MIT: the Center for Global Change Science (CGCS) and the Center for Energy and Environmental Policy Research (CEEPR). These two centers bridge many key areas of the needed intellectual work, and additional essential areas are covered by other MIT departments, by collaboration with the Ecosystems Center of the Marine Biology Laboratory (MBL) at Woods Hole, and by short- and long-term visitors to the Program. The Program involves sponsorship and active participation by industry, government, and non-profit organizations.

To inform processes of policy development and implementation, climate change research needs to focus on improving the prediction of those variables that are most relevant to economic, social, and environmental effects. In turn, the greenhouse gas and atmospheric aerosol assumptions underlying climate analysis need to be related to the economic, technological, and political forces that drive emissions, and to the results of international agreements and mitigation. Further, assessments of possible societal and ecosystem impacts, and analysis of mitigation strategies, need to be based on realistic evaluation of the uncertainties of climate science.

This report is one of a series intended to communicate research results and improve public understanding of climate issues, thereby contributing to informed debate about the climate issue, the uncertainties, and the economic and social implications of policy alternatives. Titles in the Report Series to date are listed on the inside back cover.


Ronald G. Prinn and John M. Reilly
Program Co-Directors

For more information, please contact the Joint Program Office

Postal Address: Joint Program on the Science and Policy of Global Change
77 Massachusetts Avenue
MIT E19-411
Cambridge MA 02139-4307 (USA)

Location: 400 Main Street, Cambridge
Building E19, Room 411
Massachusetts Institute of Technology

Access: Phone: +1(617) 253-7492
Fax: +1(617) 253-9845
E-mail: globalchange@mit.edu
Web site: <http://globalchange.mit.edu/>

 Printed on recycled paper

Quantifying the Likelihood of Regional Climate Change: A Hybridized Approach

C. Adam Schlosser^{**}, Xiang Gao^{*}, Kenneth Strzepek^{*}, Andrei Sokolov^{*}, Chris E. Forest[†],
Sirein Awadalla^{*}, and William Farmer[§]

Abstract

The growing need for risk-based assessments of impacts and adaptation to climate change calls for increased capability in climate projections: the quantification of the likelihood of regional outcomes and the representation of their uncertainty. Herein, we present a technique that extends the latitudinal projections of the 2-D atmospheric model of the MIT Integrated Global System Model (IGSM) by applying longitudinally resolved patterns from observations, and from climate-model projections archived from exercises carried out for the 4th Assessment Report (AR4) of the Intergovernmental Panel on Climate Change (IPCC). The method maps the IGSM zonal means across longitude using a set of transformation coefficients, and we demonstrate this approach in application to near-surface air temperature and precipitation, for which high-quality observational datasets and model simulations of climate change are available. The current climatology of the transformation coefficients is observationally based. To estimate how these coefficients may alter with climate, we characterize the climate models' spatial responses, relative to their zonal mean, from transient increases in trace-gas concentrations and then normalize these responses against their corresponding transient global temperature responses. This procedure allows for the construction of meta-ensembles of regional climate outcomes, combining the ensembles of the MIT IGSM—which produce global and latitudinal climate projections, with uncertainty, under different global climate policy scenarios—with regionally resolved patterns from the archived IPCC climate-model projections. This approach also provides a hybridization of the climate-model longitudinal projections with the global and latitudinal patterns projected by the IGSM, and can be applied to any given state or flux variable that has the sufficient observational and model-based information.

Contents

1. INTRODUCTION	2
2. METHODOLOGY	4
2.1 Analytic Formalism	4
2.2 Regional Climate-Change Transformations	7
2.2.1 Precipitation	8
2.2.2 Surface-Air Temperature	9
2.2.3 Inter-Scenario Consistency	11
3. HYBRID FREQUENCY DISTRIBUTIONS	13
3.1 Southwestern United States Region	17
3.2 Western Europe Region	19
3.3 Blue Nile Region	21
3.4 Yedoma Region	23
3.5 Amazon Region	24
3.6 Southeastern Australia Region	26
3.7 South Africa Region	27
4. CLOSING REMARKS	28
5. REFERENCES	31

* MIT Joint Program for the Science and Policy of Global Change, Cambridge, MA

† Corresponding Author: C. Adam Schlosser (email: casch@mit.edu)

‡ Dept. of Meteorology, Pennsylvania State University, State College, PA

§ Dept. of Civil Engineering, Tufts University, Medford, MA

1. INTRODUCTION

Under the growing threat of human-induced climate change and the consequent risks to natural and managed ecosystems as well as society, there is an increasing need for regionally detailed information of important atmospheric variables (e.g. temperature and precipitation). To meet this need, a number of issues must be addressed that involve: modeling and predicting a complex system such as the Earth's climate; the uncertainty of the climate response from human forcing (e.g. Forest et al., 2006); and the assurance that the computational techniques and experimentation employed faithfully portray this uncertainty (e.g. Knutti, 2010). When extending this to integrated assessments of climate change, regional climate-prediction uncertainties, in addition to other uncertain aspects of the global climate system response (e.g. Forest et al., 2006) as well as emissions and their corresponding climate policies (e.g. Webster et al., 2011) lead to an overarching issue of "climate risk", which impact and adaptation studies must encompass and incorporate in an increasingly quantifiable capacity.

To that end, previous assessment exercises have employed spatial disaggregation techniques so that changes in key inputs, such as temperature and precipitation, are provided at the necessary level of spatial detail (e.g. Yohe and Schlesinger 1998). Such class of software tools has been developed over the past two decades to provide modelers with a reduced form method to explore potential climate changes under a broader range of global greenhouse gas (GHG) emissions than provided by climate models from the Intergovernmental Panel on Climate Change (IPCC) exercises. Most of these disaggregation tools have utilized pattern-scaling methods (e.g. Santer, et al 1990) to relate global mean temperature to spatial gridded impacts on temperature and precipitation based on climate-model results. Additionally, analysis of the resulting global mean temperature over a range of climate-model parameters is desirable (e.g. Sokolov et al., 2009), and so additional techniques have involved equally probable sampling of modeled information. Some examples of these tools are the Model for the Assessment of Greenhouse-gas Induced Climate Change (MAGICC) that drives a spatial climate-change SCENario GENerator (MAGICC/SCENGEN, Wigley, 2011); the Electric Power Research Institute (EPRI) second version of Country Specific Model for Intertemporal Climate (COSMIC 2, EPRI, 2005); and the Simulator for Climate - SimCLIM (ClimSystems, 2011).

MAGICC/SCENGEN has been one of the primary model-guidance tools used within the IPCC policy/impact arena. Its climate model is an upwelling-diffusion, energy-balance model that produces global- and hemispheric-mean temperature and also estimates oceanic thermal expansion. Global-mean temperatures from MAGICC drive SCENGEN's pattern-scaling method (Santer et al., 1990) to produce spatial patterns of change in surface-air temperature and precipitation. The pattern scaling method is based on the separation of the global-mean and spatial-pattern components of future climate change from the climate model database of the IPCC's 4th Assessment Report (AR4, IPCC 2007) archive. Spatial patterns in the database are normalized and expressed as changes per 1° C change in global-mean temperature. For the SCENGEN scaling component one can use linear or power law (exponential) scaling. For

precipitation changes, exponential scaling to the global temperature response has also been applied (Hulme et al., 1995).

In another method, EPRI released its second version of COSMIC 2 in 2005 (EPRI 2005). It is similar to MAGICC/SCENGEN using dynamic global predictions of mean temperature with climate patterns predicted by 14 climate models. However, COSMIC outputs are averaged by country. The averaging can be by area weights or population weights. The climate change predictions are interpolated to 0.5° by 0.5° squares. The temperature and precipitation changes are then added and averaged for complete coverage of each country for the area-weighting scheme. The population-weighting scheme multiplies each square by the fraction of the country's population residing in the square before completing the averaging calculation (Williams et al., 1998; Schlesinger et al., 2000; Schlesinger and Malyshev, 2001).

SimCLIM is an integrated modeling system for assessing climate change impacts and adaptation that uses MAGICC and a pattern matching tool, similar to SCENGEN, with CMIP3/AR4 CGMs. It provides a number of extensions to the climate data provided by the MAGICC/GCM linkage to assist modelers to perform climate change impact and adaptation studies. These extensions include a set of global climate databases, tools for spatial interpolation of coarsely gridded climate change data, and statistical downscaling in some regions. Additional SimCLIM is part of an integrated modeling system that includes a crop model PlantGro and other biophysical impact models to provide for seamless use of historic or future climate projections with the supplied models. Additionally the modeling system is an open-framework so users can easily “integrate” their own biophysical models with the SimCLIM generated climate scenarios, (Warrick 2009, and Pulhin 2010).

Yet, what is absent from current methods is an ability to quantify the likelihood of particular regional outcomes, and that these outcomes can be generated under a consistent array of climate policies, modeled within a socio-economic framework with its underlying uncertainties, and one that can be tailored to any particular policy target. Therefore, when applied to analyses on impacts and/or adaptation to climate change, information from the aforementioned approaches is limited in scope and flexibility. In this study, we present an approach that addresses this issue by applying a regional analysis capability to the Integrated Global Systems Model IGSM (Sokolov et al. 2009). The IGSM is an earth model of intermediate complexity (EMIC) linked to a multi-sector, multi-regional model of the global economy (Paltsev et al., 2005). We present a method whereby the native frequency distributions of the IGSM outputs by latitude zones are transposed across their corresponding longitudinal grids based on a method that applies a linear expansion of climate model information at the regional detail. In the section that follows, we present this approach, which includes the construction of an observation-based climatology of the downscaling patterns as well as a normalization of the climate-model patterns of regional change. These steps are based on GCM ensemble results from the IPCC AR4. The resulting frequency distributions are evaluated for a select number of regions to assess their consistency with the inferred distributions from the more limited sample of the IPCC model collection, and further analyses evaluates the shifts in these derived distributions under a moderate climate-

stabilization policy. Closing remarks and directions for future work and applications are then provided.

2. METHODOLOGY

2.1 Analytic Formulation

The atmospheric component of the IGSM is a 2-D model in altitude and latitude, and we therefore begin by considering any latitudinal zonal (mean) field of any state or flux variable of the IGSM, \bar{V}_y^{IGSM} , at any given point in time. Our intent is to expand \bar{V}_y^{IGSM} such that we are able to describe its variation across the latitude. We can represent this transformation as:

$$V_{x,y}^{IGSM} = C_{x,y} \bar{V}_y^{IGSM} \quad (1)$$

where, $C_{x,y}$, is a transformation coefficient that corresponds to the longitudinal point (x) along any given latitude (y) and maps \bar{V}_y^{IGSM} to its corresponding longitudinal value, $V_{x,y}^{IGSM}$. While this transformation can apply, in principle, to any state or flux quantity, here the variables of interest are surface-air temperature (T_a) and precipitation (P). To calculate $C_{x,y}$ we employ the widely used observational datasets of the Climate Research Unit (CRU, Jones *et al.* 1999) and the Global Precipitation Climatology Project (GPCP) of Adler *et al.* (2007), for the T_a and P estimates, respectively. Each of these data sets is provided at monthly timesteps, and so we build the climatological description accordingly. For any given gridpoint of the CRU and GPCP data, for every month of their timeseries, we calculate:

$$C_{x,y} = \frac{V_{x,y}}{\bar{V}_y} \quad (2)$$

to obtain a timeseries of the $C_{x,y}$ coefficients. Note that the values of $C_{x,y}$ are unitless, and reflect the relative value of any given variable at a longitudinal point in relation to its zonal mean. From this, a climatology of these transformations, $\bar{C}_{x,y}$, can be evaluated from observations. For this study, we produce a monthly climatology by obtaining averages for the period 1981-2000.

For surface-air temperature (**Figure 1**), the corresponding patterns of $\bar{C}_{x,y}$ reveal an intuitively consistent seasonality. During the northern hemisphere winter, the relatively warmer regions of Western Europe and North America - as a result of persistent maritime fetch as well as the notably colder, continental climate region of Siberia and the Hudson Bay region - are clearly distinguished. Further, warmer regions in the interior continents (e.g. Eurasia and Australia) during summer are well represented, as are the persistently cooler high elevations as well as warmer desert regions are also clearly seen.

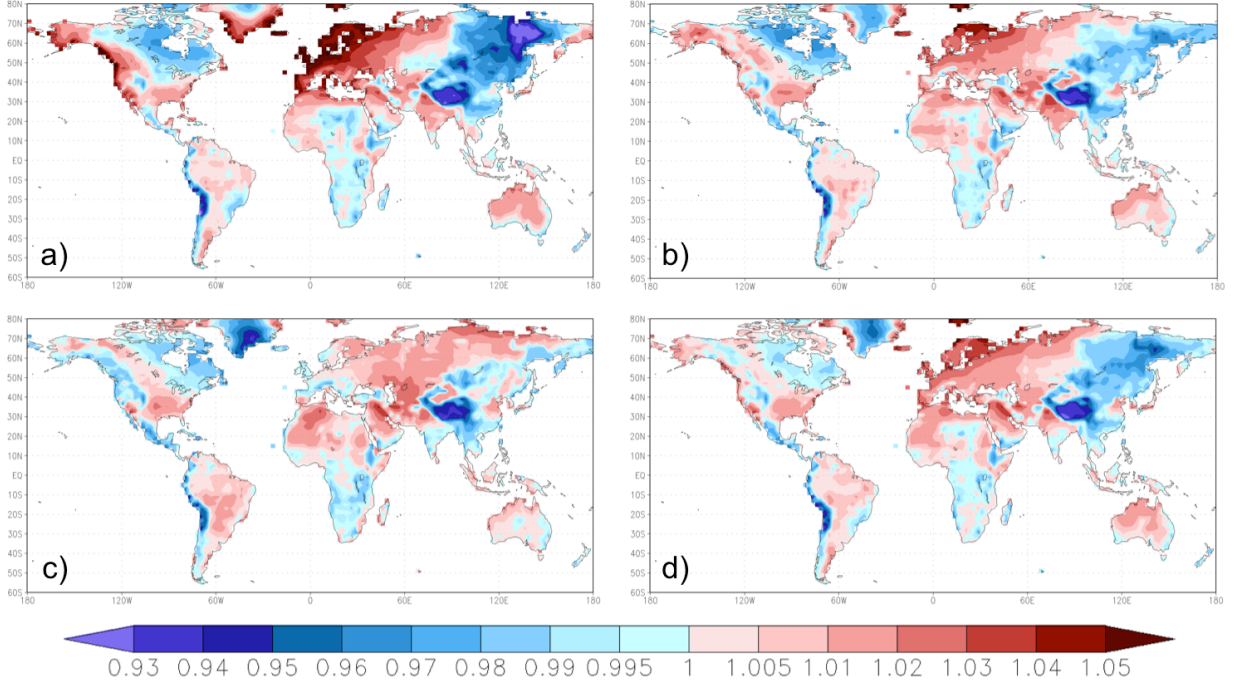


Figure 1. Global maps of the transformation coefficients, $\bar{C}_{x,y}$, (unitless) for surface-air temperature based on observations from the Climate Research Unit (CRU). Seasonally averaged results (1981-2000) shown for: a) December-February, b) March-May, c) June-August, and d) September-November.

For precipitation (**Figure 2**), we similarly find that the technique produces intuitively consistent and characteristic depictions of the global structure of precipitation. For example, the enhanced precipitation regions associated with the preferential location of storm tracks along the western boundary of the Atlantic and Pacific oceans are evident. In addition, the widespread desert regions are also clearly seen throughout the entire year and the progression of the Inter-Tropical Convergence Zone (ITCZ) is also captured.

Given these climatological constructions, we then apply this transformation to account for potential shifts or changes in climate, and therefore consider that the transformation coefficients, $C_{x,y}$, may change, in a characteristic fashion, as the global system climate changes. We then expand (1) to a more comprehensive expression as a first-order (i.e. linear) Taylor expansion with respect to global temperature change (ΔT_{Global}). Thus, the IGSM zonal transformation process as global temperature varies can therefore be written as:

$$V_{x,y}^{IGSM}(\Delta T_{Global}) = C_{x,y}|_{T_0} \bar{V}_y^{IGSM} + \left[\frac{dC_{x,y}}{dT_{Global}} \Delta T_{Global} \right] \bar{V}_y^{IGSM} \quad (3)$$

where $C_{x,y}|_{t_0}$ is the transformation coefficient for any reference time period, and in our case, we can equate this to the aforementioned climatological set of values, $\bar{C}_{x,y}$, based on observational

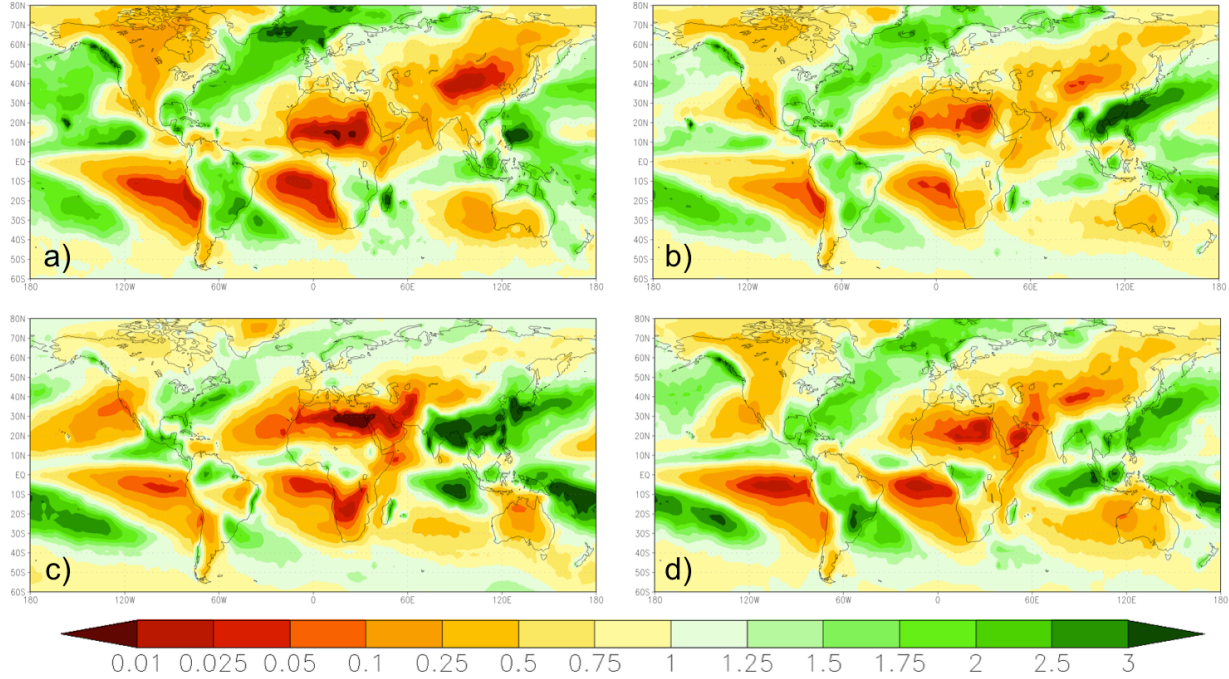


Figure 2. Global maps of the transformation coefficients, $\bar{C}_{x,y}$, (unitless) for precipitation based on observations from the Global Precipitation Climatology Project (GPCP). Seasonally averaged results (1981-2000) shown for: a) December-February, b) March-May, c) June-August, and d) September-November.

data. Accordingly, ΔT_{Global} is the change in global temperature that has occurred relative to the reference or climatological period. Then, based on supporting data the derivative of these transformation coefficients, $\frac{dC_{x,y}}{dT_{Global}}$, for any point (x,y) must be estimated. For this construction,

we are particularly interested in how these transformation coefficients may vary as a result of any human-forced global temperature change. In the section that follows, the transformation coefficient derivatives are constructed from a suite of IPCC scenarios from the AR4 archive. In doing so, we continue our focus of this technique on two variables of interest: surface-air temperature and precipitation. Evaluations are then made as to whether the derivatives represent a characteristic response in the IPCC climate-model collection.

2.2 Regional Climate-Change Transformations

Applying the construction above, the derivative of the transformation coefficients, $\frac{dC_{x,y}}{dT_{Global}}$, will be estimated from GCM climate simulations forced by the scenarios from the IPCC Special

Report on Emission Scenarios (SRES) as well as from the transient CO₂ increase simulations (2xCO₂) performed by the climate model community in support of the IPCC AR4. These multi-model and multi-scenario sets of data provide an opportunity to assess whether simulated shifts are robust (across emission scenarios), and also to assess their structural uncertainty (across all the climate models). To calculate these terms, we draw results from this model population to calculate the shifts in $C_{x,y}$ between a beginning (t_0) and ending (t_1) point in time:

$$\frac{dC_{x,y}}{dT} = \frac{\overline{C}_{x,y}^{t_1} - \overline{C}_{x,y}^{t_0}}{\overline{T}_{Global}^{t_1} - \overline{T}_{Global}^{t_0}} \quad (4)$$

The choice of t_0 and t_1 is somewhat arbitrary, but should span a sufficient amount of time such that a climate response (if any) has evolved as a result of the trends in the trace-gas forcing. For the scenarios considered herein, we chose t_0 and t_1 to span the number of years at which a doubling of CO₂ at a transient rate of 1% per year has been achieved, equivalent to 70 years. The overbars denote that average values, at t_0 and t_1 , are taken for the calculation and we used a 10-year averaging period, starting at each reference time, t_0 and t_1 ¹. Further, the results are temporally resolved at a monthly timestep, and therefore we produce a monthly climatology (based on the difference of their 10-year means) of these transformation coefficients of regional climate change. From the IPCC archive, three SRES scenarios are considered for these calculations: the A2 scenario (17 climate models), the A1B scenario (17 climate models), and the B2 scenario (17 climate models). The transient 2xCO₂ simulation also provides an additional collection of 19 climate model simulations from the IPCC AR4. We first consider the results from the A2 SRES scenario and assess the multi-model mean and scatter (standard deviation) of $\frac{dC_{x,y}}{dT_{Global}}$ for precipitation and surface-air temperature. In the analysis that follows, all the climate model results have been bi-linearly interpolated to a common 2°x2° resolution grid prior to any calculations made.

2.2.1 Precipitation

The model-mean of $\frac{dC_{x,y}}{dT_{Global}}$ for precipitation (**Figure 3**) indicates a swath of drier conditions, relative to the zonal mean, as a result of climate warming that extends from the central, subtropical North Pacific into the European continent and North Atlantic. Along this swath, an enhanced area of relative drying is seen over Central America and Western Europe. While this drying persists in these regions throughout most of the year, it is strongest during the warmer months. A similar feature is also prominent in the South Pacific basin, and extends over the southernmost tip of South America and persists for all seasons with an enhancement over

¹ For these calculations, the averaging periods are 2000-2010 and 2070-2080.

Patagonia and southern Argentina. The most prominent land areas of relatively wetter conditions occur over the Asian monsoon region.

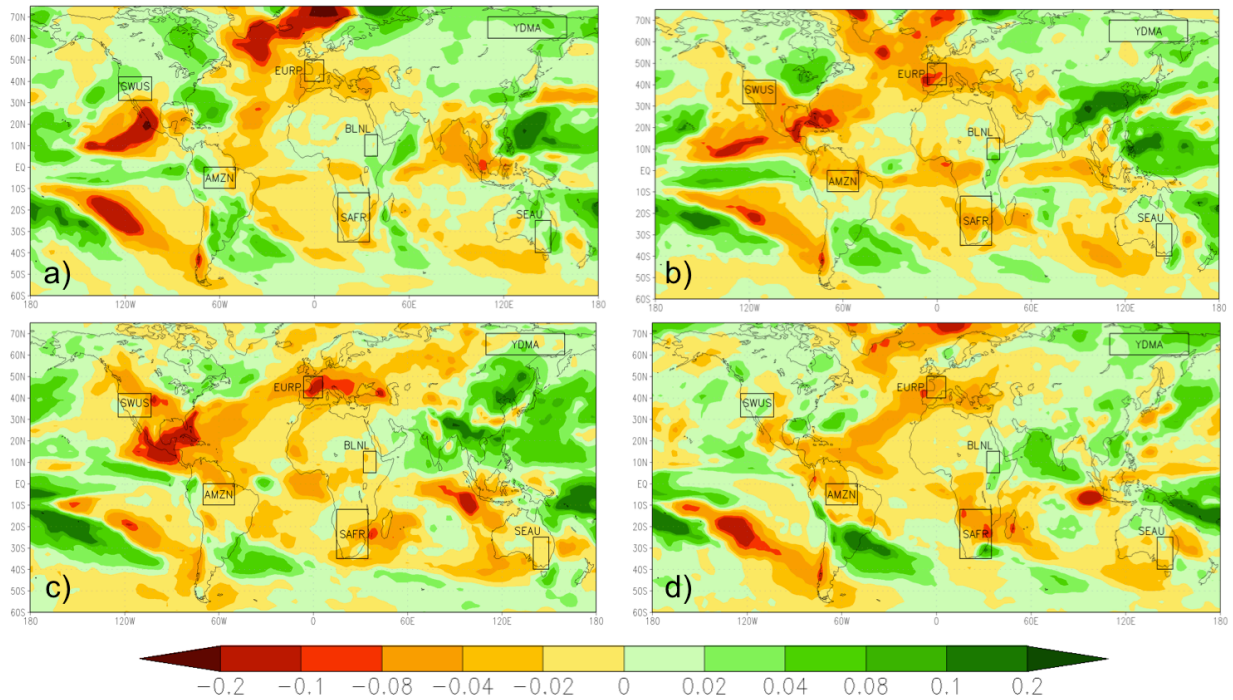


Figure 3. Global maps of the transformation coefficients, $dC_{x,y}/dT_{Global}$ (units of K^{-1}) for precipitation based on the IPCC AR4 climate models. Shown are the model-mean, seasonally averaged results for: a) December-February, b) March-May, c) June-August, and d) September-November.

Generally speaking, higher degrees of scatter amongst the models in $\frac{dC_{x,y}}{dT_{Global}}$ for precipitation (Figure 4) are prevalent over the world's oceans, most notably in the subtropical Pacific, the western boundary of the North Atlantic, and tropical Atlantic. The most extensive regions of this large scatter are found in the oceanic subtropical regions during winter and spring. Over land, the Indian and southeast Asian monsoon regions display the largest degree of model scatter. Other notable land areas indicating a high degree of model scatter (i.e. comparable to the mean values in Figure 3) include the eastern half of North America, most of Central America, and northern half of South America. A large portion of Eurasia and North Africa contain the lowest values of the inter-model deviations, particularly during the colder seasons.

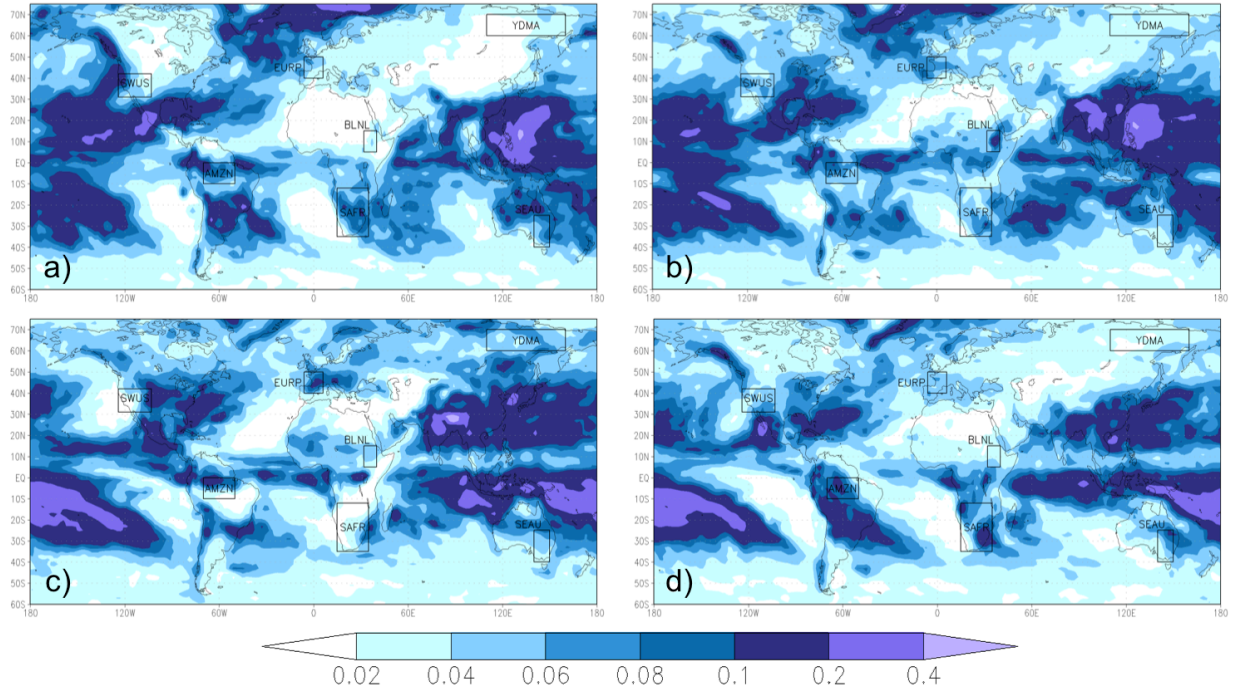


Figure 4. Global maps of the standard deviation of the transformation coefficients, $dC_{x,y}/dT_{Global}$ (units of K^{-1}) for precipitation across the IPCC AR4 climate models. Shown are the seasonally averaged results for: a) December-February, b) March-May, c) June-August, and d) September-November.

2.2.2 Temperature

The most striking feature of the model-mean $\frac{dC_{x,y}}{dT_{Global}}$ for T_a (**Figure 5**) is the resemblance of the colder ocean and warmer land (COWL) global pattern (e.g. Broccoli *et al.*, 1998) global pattern seen in all seasons. The most notable exceptions to this characterization lie in the northernmost regions of the northern hemisphere land areas. Over northern Siberia, the relative cooling signal is most likely a result of thermal inertia from the snow pack and frozen soil conditions (if the climate models' soil physics resolve this explicitly). Conversely, over the coastal regions of North America, the maritime fetch of the relatively cooler ocean conditions has a large influence. This maritime influence is also notable in winter over Europe, the southern half of South America, as well as southeastern United States. Relatively speaking, land regions where some of the largest warming occurs include South Africa, West Africa, the Himalayan region, and the greater Hudson Bay basin. With the exception of the aforementioned relative cooling from the maritime fetch during the winter, no discernable seasonal features to the warming patterns over land are discernable.

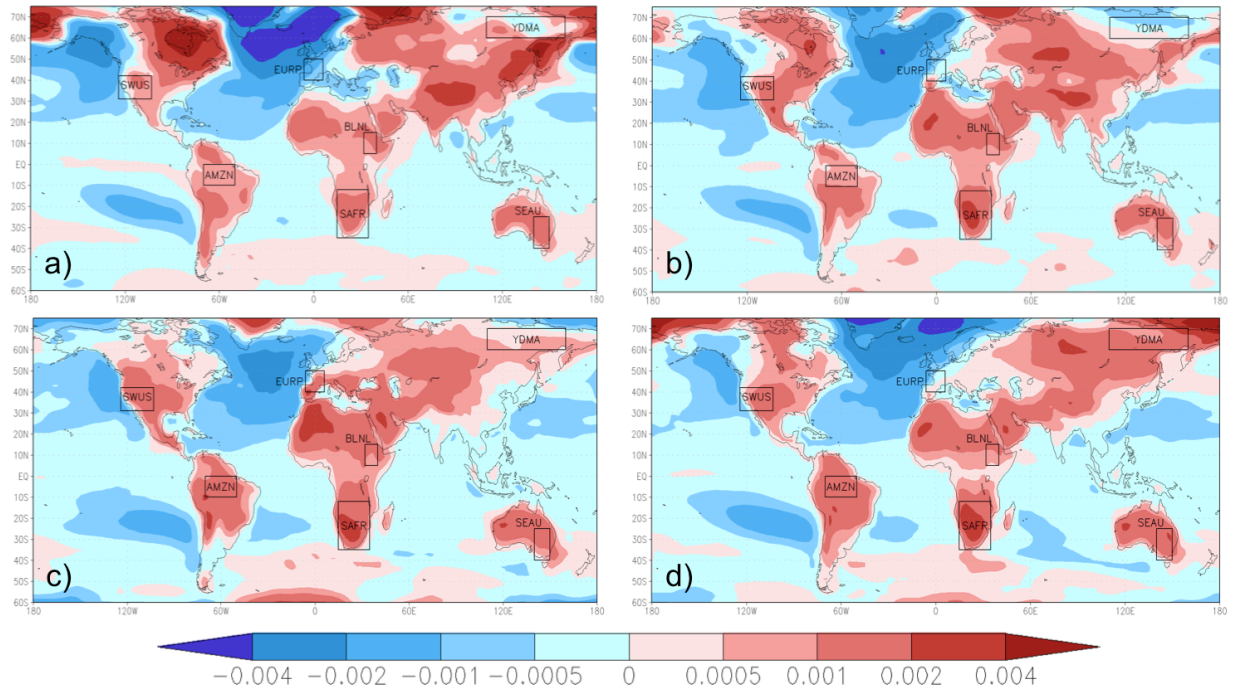


Figure 5. Global maps of the transformation coefficients, $dC_{x,y}/dT_{Global}$ (units of K^{-1}) for surface-air temperature based on the IPCC AR4 climate models. Shown are the model-mean, seasonally averaged results for: a) December-February, b) March-May, c) June-August, and d) September-November.

Scatter amongst the models in $\frac{dC_{x,y}}{dT_{Global}}$ for T_a (**Figure 6**) indicate ubiquitously elevated values covering the boreal region of the Northern Hemisphere, most notably during the winter and spring seasons. Other isolated regions of higher inter-model scatter occur over interior portions of South America, Australia, the Sahel, and South Africa. Contrary to the model scatter in precipitation, the lowest values of model scatter occur over much of the world's ocean, with the lowest values confined to the subtropics. Moreover, there are no striking features in the seasonality of the oceanic minima. Conversely, the widespread maxima of model scatter in the northern hemisphere show their southernmost extent during the winter and northernmost retreat in the fall. Generally speaking, land regions indicated by shades of darkest blue and purple (i.e. $> 0.001 K^{-1}$) are regions where the inter-model scatter is equal to or exceeding that of the model-mean value of $\frac{dC_{x,y}}{dT_{Global}}$. The coincidence of large model scatter with respect to the model-mean response has important implications to the resultant regional frequency distributions that are constructed from the (zonal) IGSM ensemble simulations, which are presented in Section 3.

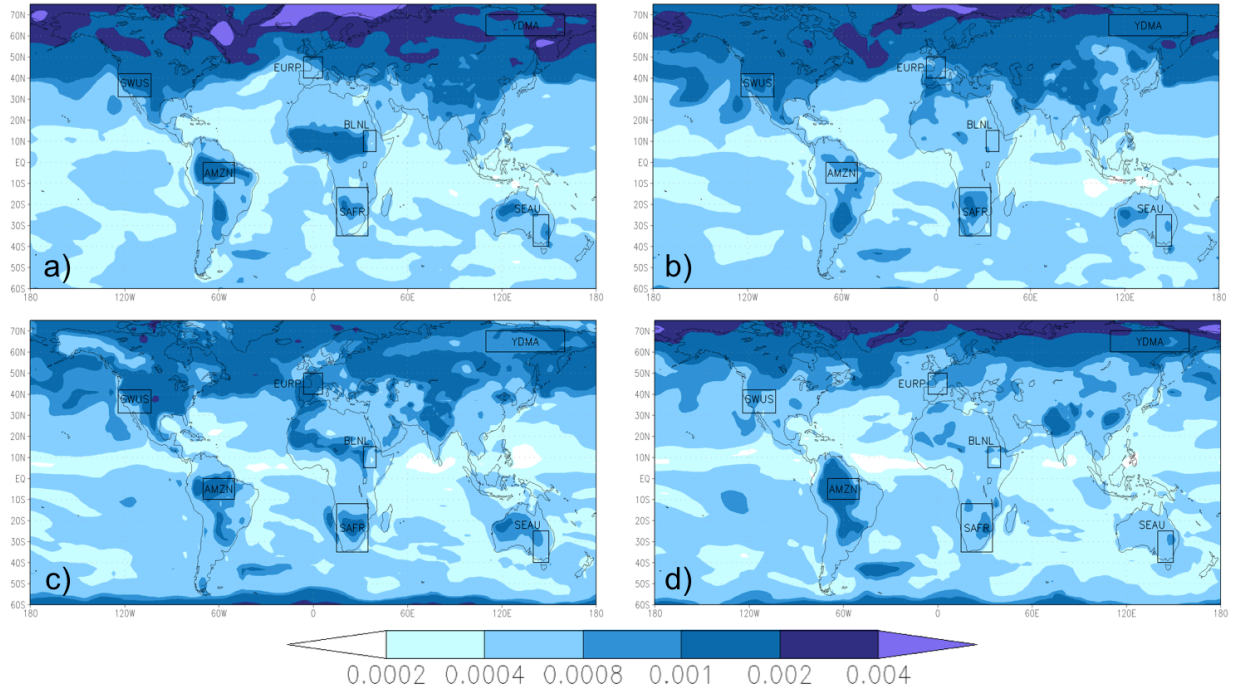


Figure 6. Global maps of the standard deviation of the transformation coefficients, $dC_{x,y}/dT_{Global}$ (units of K^{-1}) for precipitation across the IPCC AR4 climate models. Shown are the seasonally averaged results for: a) December-February, b) March-May, c) June-August, and d) September-November.

2.2.3 Inter-Scenario Consistency

The results presented in the previous section for the $\frac{dC_{x,y}}{dT_{Global}}$ estimates were derived from the climate-model simulations of the SRES A2 scenarios. Although this calculation involves a normalization of the pattern changes with respect to a unit increment of global temperature, the issue remains as to whether these (normalized) changes are robust across simulated climate projections under different GHG emission scenarios. To explore this question, we calculated the same suite of $\frac{dC_{x,y}}{dT_{Global}}$ metrics for the A1B and B2 scenarios as well as for the 2xCO₂ experiment, and obtained seasonally averaged maps of these quantities similar to those in Figures 3 to 6. If the climate-model responses are robust across these scenarios, we should expect a high degree of spatial consistency among their corresponding $\frac{dC_{x,y}}{dT_{Global}}$ results. To quantify this relation, we calculated for all seasons the spatial correlation for the model-mean global fields of $\frac{dC_{x,y}}{dT_{Global}}$ between all possible combinations of SRES and 2xCO₂ scenarios. This spatial correlation calculation is then repeated using the inter-model standard deviation of $\frac{dC_{x,y}}{dT_{Global}}$.

Table 1. Spatial correlations between the global patterns of $dC_{x,y}/dT_{Global}$ from the AR4 scenarios considered in this study (A2, A1B, and B2). Results are presented for surface-air temperature and precipitation coefficients. The spatial correlations between the mean (T_{mean} and P_{mean}) and standard deviation (T_{std} and P_{std}) amongst the AR4 models' $dC_{x,y}/dT_{Global}$ patterns. Results are provided for annual averages as well as for four seasonal periods: December-February (DJF), March-May (MAM), June-August (JJA), and September-November (SON).

	A2 vs. A1B				A2 vs. B1				A1B vs. B1			
	T_{mean}	P_{mean}	T_{std}	P_{std}	T_{mean}	P_{mean}	T_{std}	P_{std}	T_{mean}	P_{mean}	T_{std}	P_{std}
DJF	0.98	0.84	0.96	0.80	0.97	0.82	0.95	0.77	0.98	0.83	0.97	0.78
MAM	0.98	0.85	0.96	0.80	0.97	0.82	0.94	0.73	0.98	0.81	0.96	0.72
JJA	0.98	0.90	0.97	0.84	0.96	0.79	0.91	0.72	0.96	0.82	0.91	0.76
SON	0.99	0.80	0.98	0.76	0.97	0.79	0.95	0.76	0.98	0.81	0.96	0.76
Annual	0.99	0.89	0.98	0.82	0.98	0.88	0.96	0.80	0.99	0.88	0.97	0.81

The results (**Table 1**) indicate that a high degree of spatial consistency is maintained for all seasons and between all SRES scenarios considered. This consistency is remarkably high for the surface-air temperature results, with all correlations for the model-mean patterns at or above 0.96, and only a slight degradation in the correlations of the inter-model standard deviation patterns with all values at or above 0.91. For precipitation, the spatial correlations of the model-mean results among all the scenarios (and seasons) are still impressive with values at or above 0.79. Similar to the results for T_a , a slight degradation in the results for the inter-model standard deviation is seen, but values are still at or above 0.72.

Table 2. As in Table 1, but based on the AR4 simulations of $2xCO_2$ experiment compared against the A2, A1B, and B1 SRES scenarios.

	$2xCO_2$ vs. A2				$2xCO_2$ vs. A1B				$2xCO_2$ vs. B1			
	T_{mean}	P_{mean}	T_{std}	P_{std}	T_{mean}	P_{mean}	T_{std}	P_{std}	T_{mean}	P_{mean}	T_{std}	P_{std}
DJF	-0.02	0.71	0.50	0.70	0.03	0.73	0.50	0.65	0.05	0.63	0.50	0.63
MAM	0.19	0.61	0.40	0.56	0.22	0.68	0.40	0.57	0.23	0.56	0.40	0.46
JJA	0.93	0.74	0.86	0.65	0.93	0.71	0.86	0.64	0.90	0.61	0.80	0.54
SON	0.96	0.76	0.92	0.73	0.96	0.75	0.93	0.70	0.94	0.66	0.91	0.64
Annual	0.85	0.85	0.76	0.78	0.86	0.84	0.77	0.75	0.84	0.79	0.74	0.70

Looking at the results that include the $2xCO_2$ simulations (**Table 2**), one important caveat is revealed by the substantial decreases seen in the correlations during the DJF and MAM periods. The decreases are most prominent for surface-air temperature, as seen in the model-mean DJF $\frac{dC_{x,y}}{dT_{Global}}$ results for T_a from the $2xCO_2$ results (**Figure 7**). The largest discrepancy between the $2xCO_2$ results and any SRES result (Figure 5a shows the result for the A2 scenario) occurs in the northern hemisphere. The most likely cause of this result is that markedly different snow/ice albedo feedback effects are at play (both over land and ocean points) between the two

simulations. Whatever the exact cause, the important caveat here is that while the SRES scenarios are consistent in their portrayal of the $\frac{dC_{x,y}}{dT_{Global}}$ metrics, the 2xCO₂ cannot be pooled with these results. An additional point to be raised here is that regardless of these Northern Hemisphere wintertime discrepancies noted, all the simulations become consistent (high correlations) for the JJA and SON periods, particularly for the T_a results. This suggests that the warm-season patterns of $\frac{dC_{x,y}}{dT_{Global}}$ are largely insensitive to preceding wintertime conditions.

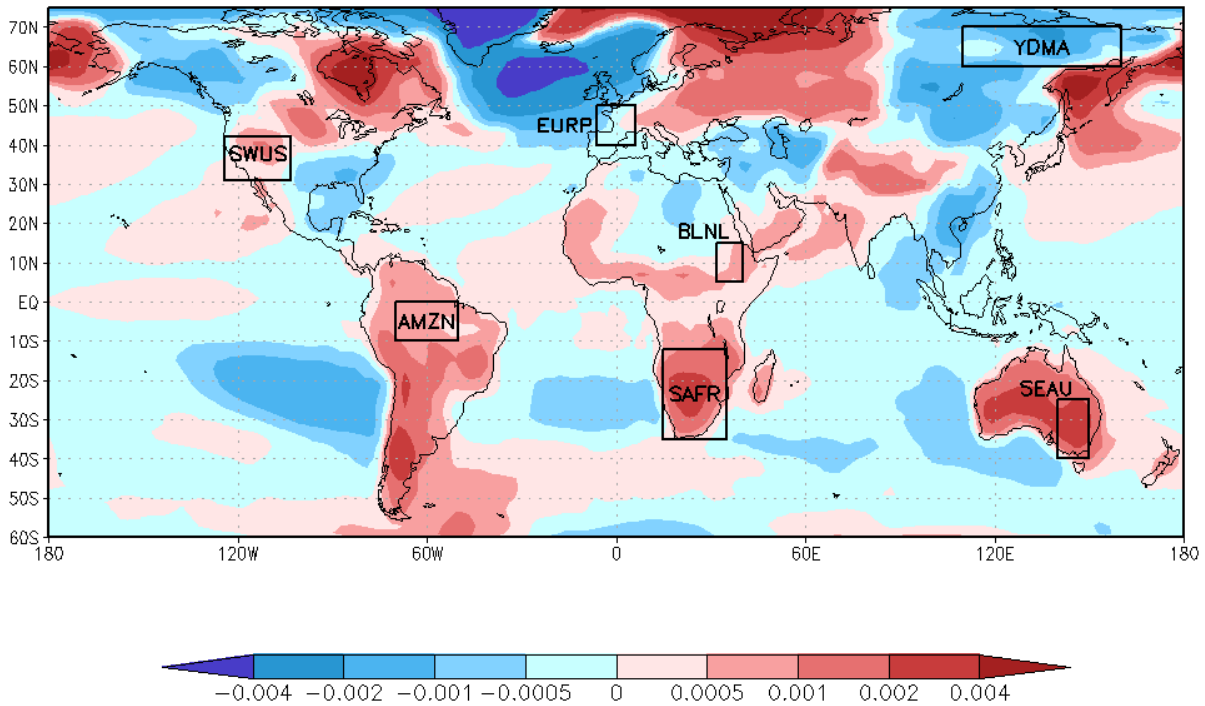


Figure 7. Global map of the transformation coefficients, $dC_{x,y}/dT_{Global}$ (units of K^{-1}) for surface-air temperature based on the 2xCO₂ experiment of the AR4 climate models. Shown is the model-mean, seasonally averaged result for December-February.

3. HYBRID FREQUENCY DISTRIBUTIONS

Given the suite of $\frac{dC_{x,y}}{dT_{Global}}$ values for both precipitation and T_a , we have a set of regional climate-change kernels with which to build a meta-ensemble by downscaling IGSM ensemble simulations (e.g. Sokolov *et al.*, 2009 and Webster *et al.*, 2010) according to (3). However, before undertaking this construction, we first assess the ability of the IGSM to faithfully portray the zonal trends in T_a and precipitation. Previous work (Sokolov *et al.*, 2010) has demonstrated

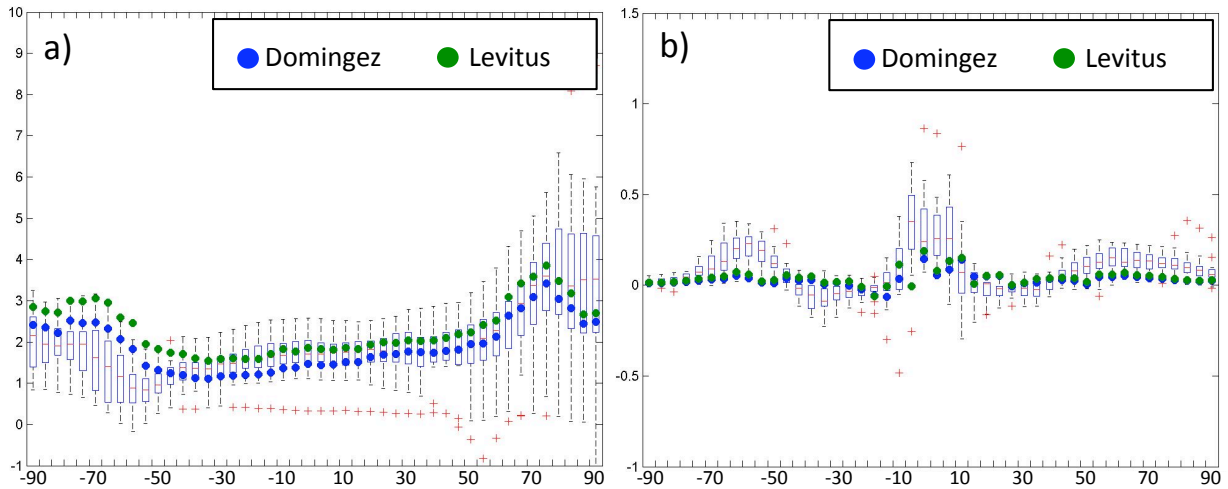


Figure 8. Zonal profiles of a) surface-air temperature (units in $^{\circ}\text{K}$), and b) precipitation (units in mm/day) change in response to a transient doubling of CO_2 concentrations. Shown are decadal mean changes between the beginning and ending period of CO_2 doubling from the IGSM as a result of two different calibrations (Sokolov *et al.*, 2010) with ocean heat-content data (blue and green dots). These are compared against the results from the IPCC AR4 climate models and presented as whisker plots (red line is the median, boxed area is the inter-quartile range, dashed line spans min and max values, and red cross-hairs denote “outliers”, which is a value that is more than 1.5 times the inter-quartile range away from the top or bottom of the box). The AR4 results presented are zonally averaged to the consistent resolution as the IGSM (4 degree latitude band widths).

that the IGSM stabilization scenarios produce global results that are aligned with the AR4 SRES scenarios from climate models. Herein, we consider how consistent the IGSM’s zonal profiles of temperature and precipitation change are with the AR4 models – using a transient doubling of CO_2 as a test case.

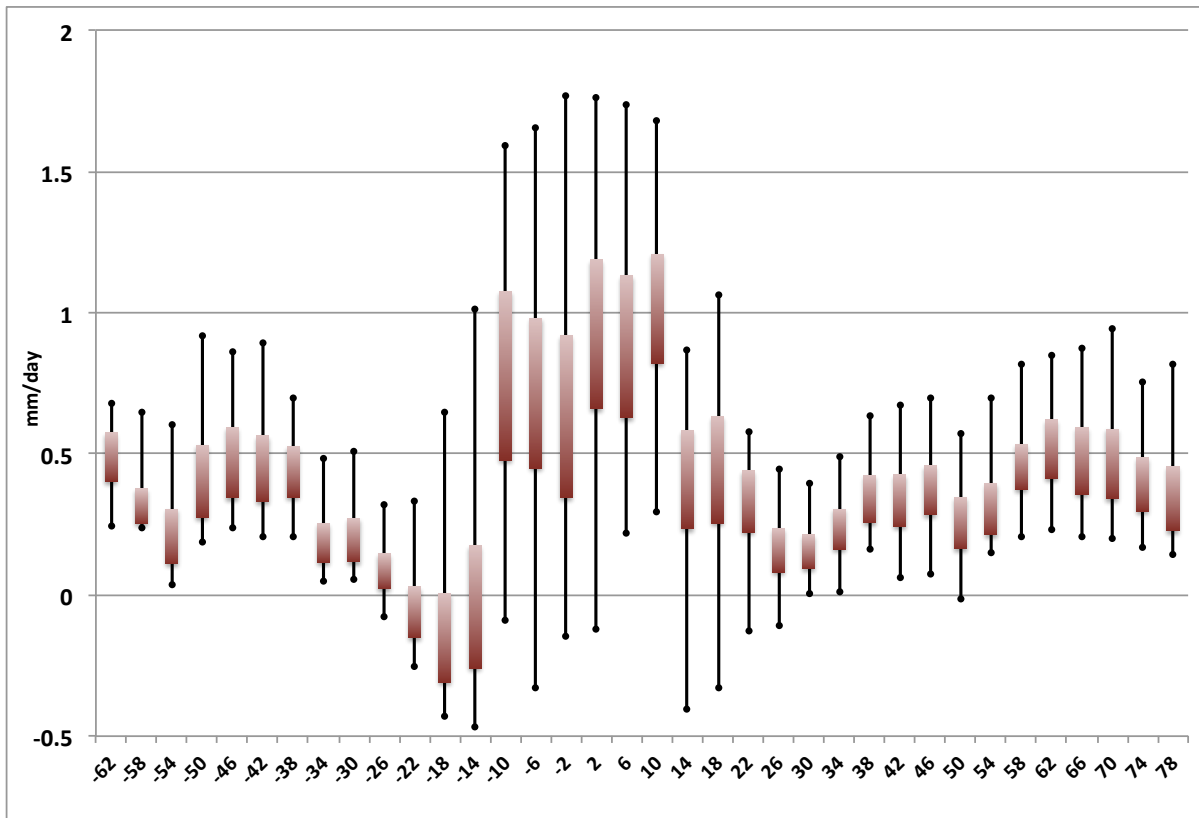


Figure 9. Zonal profiles of precipitation change (units in mm/day) in response to a transient doubling of CO₂ concentrations. Shown are decadal mean changes between the beginning and ending period of CO₂ doubling from the 400-member ensemble of the IGSM from the no-policy scenario (Sokolov *et al.*, 2010). Results are presented as whisker plots, with the endpoints denoting the minimum and maximum values, and the boxed area showing the 2 standard-deviation range centered about the median value. Latitude (in degrees) is provided in the abscissa.

Figure 8a shows the results with the application uncertainty parameters based on two separate ocean data sets, Dominguez and Levitus (for discussion see Sokolov *et al.* 2010). They reveal that the IGSM's change (increase) of annual-averaged, zonal T_a is well within the range of the AR4 climate models' responses. In all but the southernmost latitudes, the IGSM falls within the inter-quartile AR4 range, and in those exceptions the IGSM response still lies within the minimum/maximum model responses. For precipitation (**Figure 8b**), the IGSM's change in annual-averaged, zonal precipitation lies within the full range of values from the AR4 models, yet the ubiquitous inter-quartile consistency, seen in the results for T_a , is absent. The AR4 results show that for many latitude bands, the sign of the zonal precipitation change can be positive or negative, and the IGSM result shows no discernable tendency in its agreement with the majority of climate models' sign in this regard.

Overall, compared to the majority of the AR4 models, the IGSM displays smaller magnitudes of precipitation change in this 2xCO₂ scenario considered, which would characterize the IGSM's zonal precipitation response (to a change in radiative forcing) as being buffered compared to the central tendency (i.e. median) of the climate-model response, yet still consistent within the range

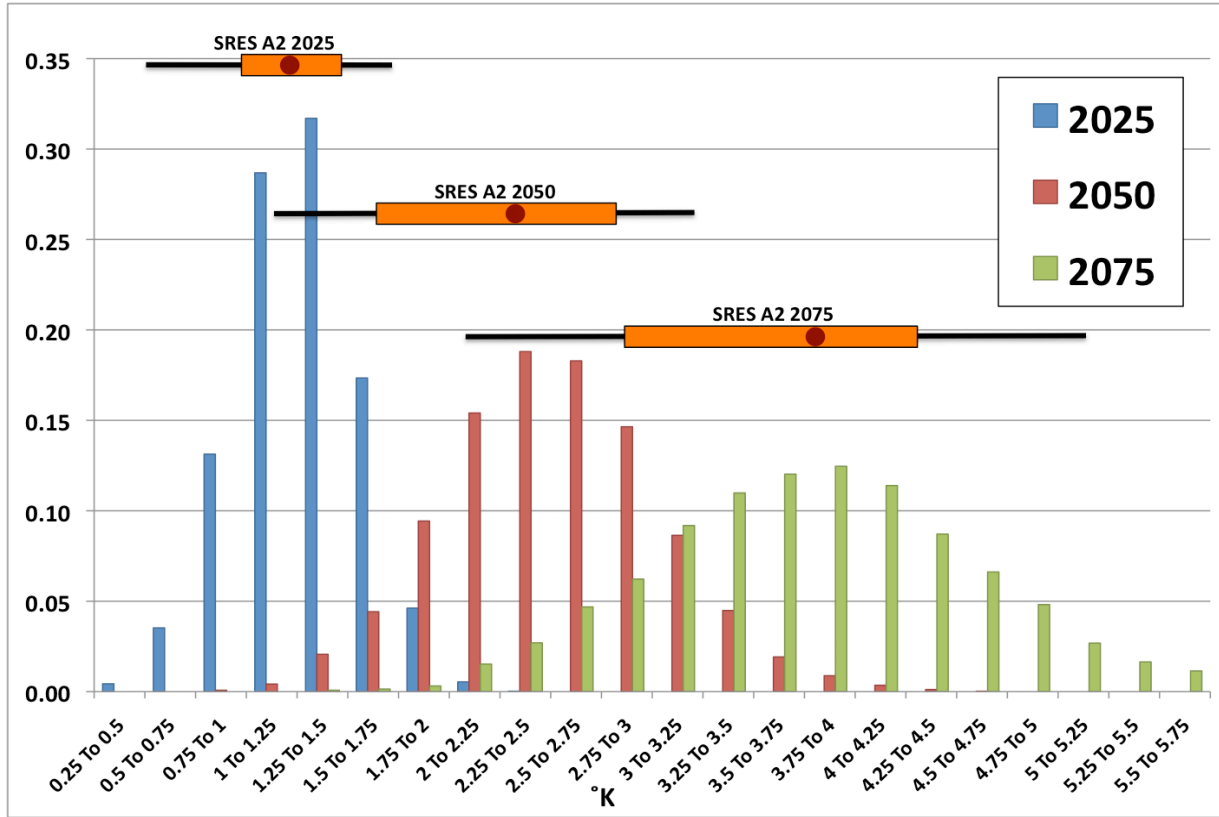


Figure 10. Hybrid frequency distributions (HFDs) of decadal averaged surface-air temperature (T_a) change (with respect to the last decade of the 20th century). The changes are area averaged for the southwestern United States (SWUS) region (boxed region denoted in Figures 3-7). Shown are the decadal averaged results starting at 2025, 2050, and 2075 from the no-policy IGSM ensemble simulation. Also denoted in the figure by the whisker plot are summaries of the climate-model decadal T_a changes at the corresponding HFD time periods from the A2 scenario of the IPCC AR4. The red circle indicates the median, the boxed region indicates the inter-quartile range, and the black line spans the minimum and maximum change.

of plausible climate model responses. However, the IGSM ensemble’s range of zonal anomalies (**Figure 9** shows results for the no-policy scenario of Sokolov *et al.*, 2010) does span a very consistent range to that seen in Figure 8 for the AR4 GCMs. We have performed this analysis with respect to seasonally averaged quantities (not shown), which results in further support that we can consider IGSM’s zonal climate response to be aligned with the AR4 model ensemble.

Given the lack of substantial inconsistencies in the IGSM’s zonal climate response as compared to the AR4 climate model collective, we next explore the use of (3) in constructing regionally downscaled projections. From the IGSM results of Sokolov *et al.* (2009) and Webster *et al.* (2011), we take all 400-members of each policy ensemble as well as the no-policy ensemble and apply these to each set of $\frac{dC_{x,y}}{dT_{Global}}$ from each of the climate models. Therefore, for the case in which we have 17 AR4 climate model results to draw from, such as the A2 scenario,

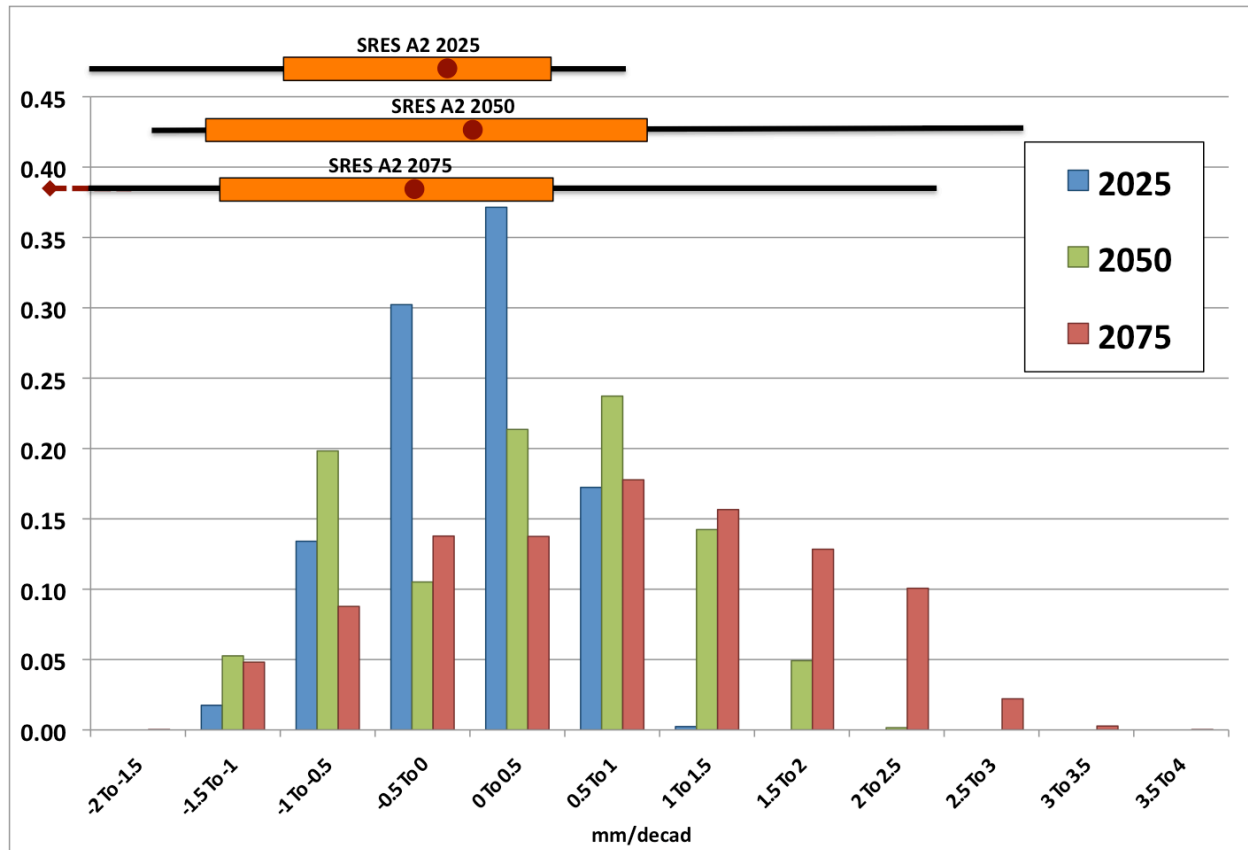


Figure 11. Hybrid frequency distributions (HFDs) of decadal averaged precipitation change (with respect to the last decade of the 20th century). The changes are area averaged for the southwestern United States (SWUS) region (boxed region denoted in Figures 3-7). Shown are the decadal averaged results starting at 2025, 2050, and 2075 based on the meta-ensemble from the spatial downscaling technique of the no-policy IGSM ensemble simulation. Also denoted in the figure by the whisker plots are summaries of the climate-model decadal precipitation changes at the corresponding HFD time periods from the A2 scenario of the IPCC AR4. The red circle indicates the median, the boxed region indicates the inter-quartile range, and the black line spans the minimum and maximum change. For the 2075 case, the minimum value (-3.2 mm/decad) extends beyond the abscissa range and is denoted by the dashed red line.

we then assume that inter-model differences within the AR4 ensembles constitute an approximate (perhaps minimal) representation of uncertainty in the longitude translation, and this procedure produce a meta-ensemble of 6,800 members. This meta-ensemble can then be treated as a hybrid frequency distribution (HFD) that integrates the uncertainty in the IGSM ensemble and in the (normalized) climate-model ensemble of regional changes.

In the next section, we apply (3) to the monthly zonal outputs of T_a and precipitation to then obtain global maps of these fields. As previously mentioned (Section 2.2), all the downscaled results are projected onto a common $2^\circ \times 2^\circ$ resolution. While this is not necessarily a requirement

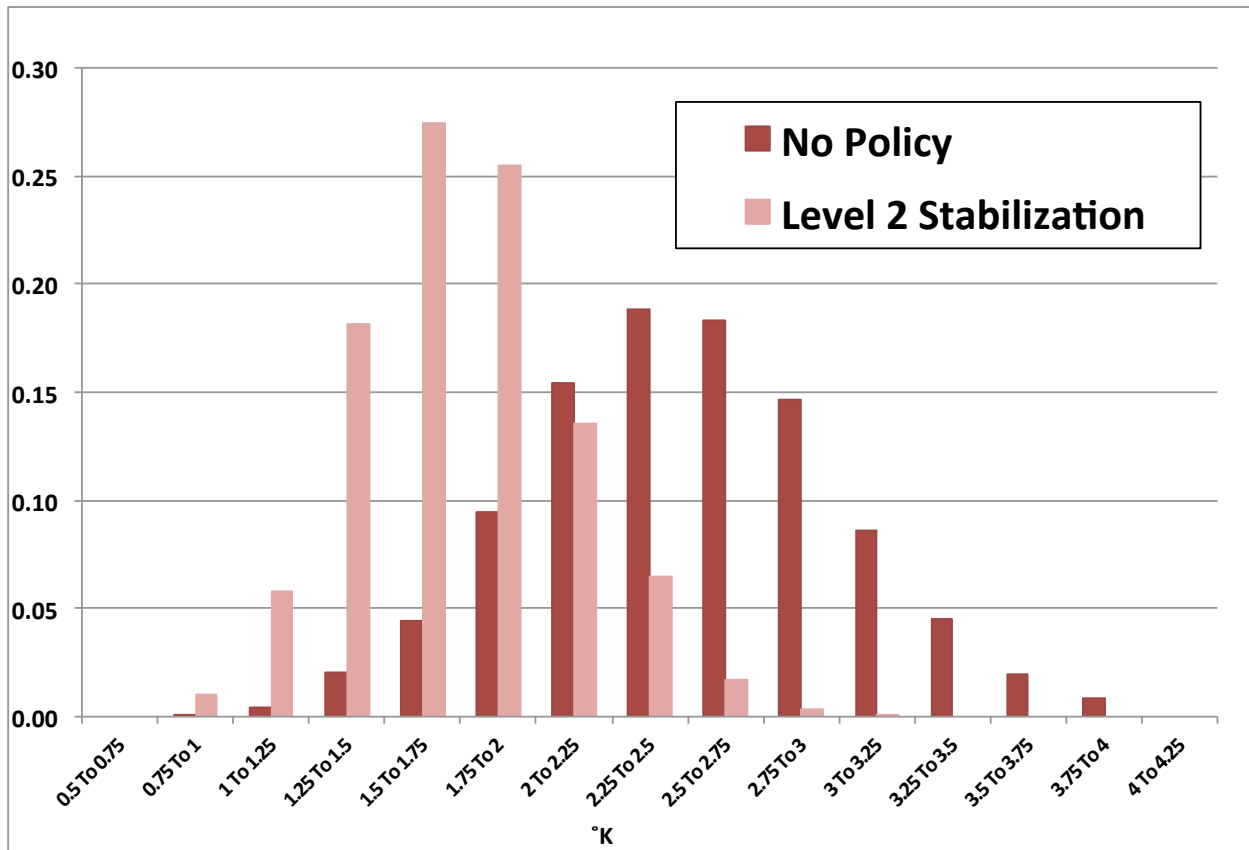


Figure 12. Hybrid frequency distributions (HFDs) of decadal averaged surface-air temperature (T_a) change (with respect to the last decade of the 20th century). The changes are area averaged for the southwestern United States (SWUS) region (boxed region denoted in Figures 3-7). Shown are the decadal averaged results starting at 2050, based on the no-policy IGSM ensemble simulation (dark red bars) and the Level 2 stabilization scenario (light red bars).

for this technique, or for the use of the resulting meta-data, it provides a common (global) gridded domain for regional analysis. In the sub-sections that follow we construct HFDs based on area-weighted averages over selected regions of the globe. Results presented for these regions serve to highlight the interpretive capabilities of the HFDs. They also demonstrate how policy can affect these HFDs and the extent to which changes in the HFDs can be inferred as representing the odds of climate change for the region. In addition, for certain regions we compare and evaluate the degree to which these HFDs convey complementary and/or consistent diagnoses to those attributed exclusively to the AR4 model results. The sub-areas selected for detailed presentation are shown in Figures 3 through 7.

3.1 Southwestern United States (SWUS)

Recent attention has been paid to the southwestern region of the United States in light of recent AR4 results, which indicate a consensus among climate models in drying out the region as a result of human-induced warming and, for some models, enhanced by insufficient increases in

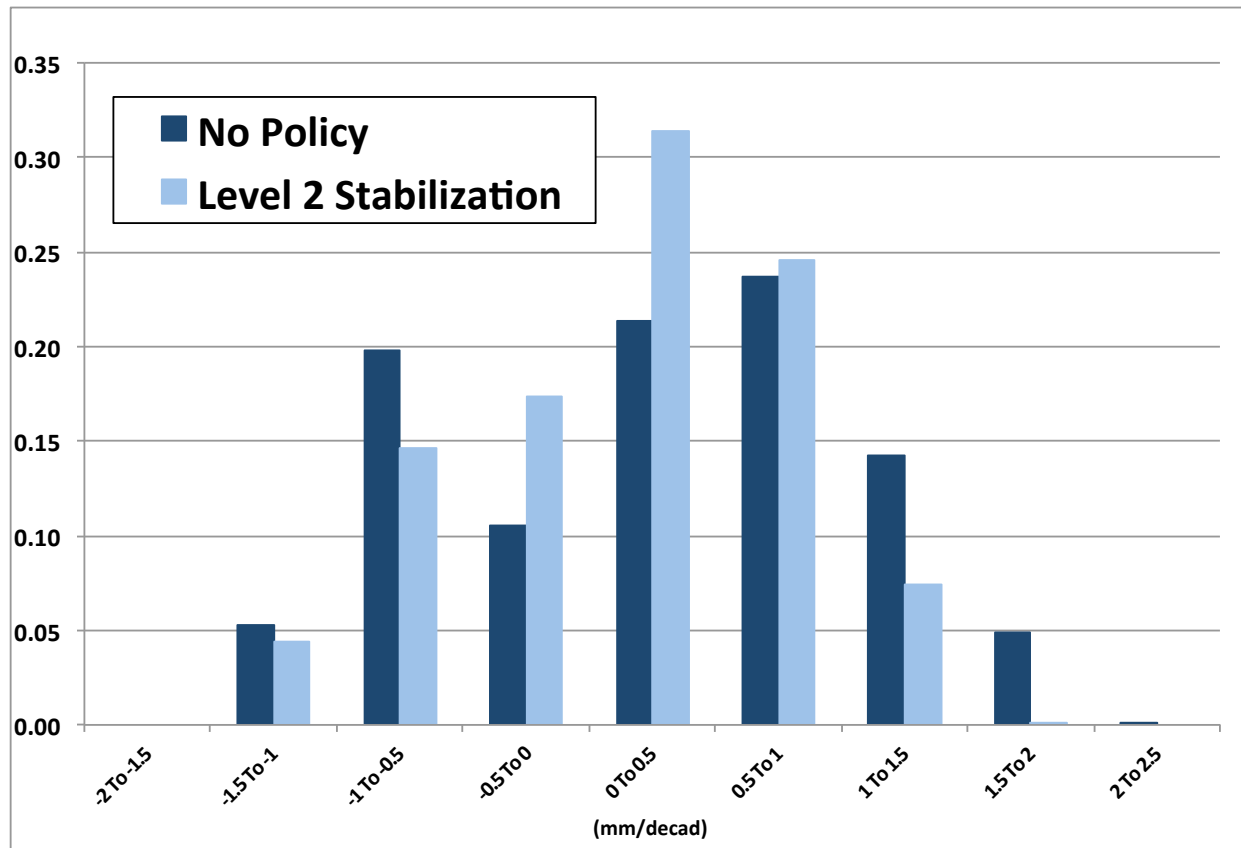


Figure 13. Hybrid frequency distributions (HFDs) of decadal averaged precipitation change (with respect to the last decade of the 20th century). The changes are area averaged for the southwestern United States (SWUS) region (boxed region denoted in Figures 3-7). Shown are the decadal averaged results starting at 2050, based on the no-policy IGSM ensemble simulation (dark blue bars) and the Level 2 stabilization scenario (light blue bars).

precipitation over the region (e.g. Seager *et al.*, 2007). Looking at the no-policy case of the downscaled IGSM meta-ensemble, the resulting HFDs of area-averaged T_a changes over time (**Figure 10**) indicate a steady warming in the mode of the distribution, reaching 3.75-4 °K by the penultimate decade of the 21st century. The HFDs further indicate that the region will most likely experience a 1° warming by 2030, but very little chance of that warming to exceed 2 °K. Moving into the middle of the 21st century, the width of the HFD nearly doubles, ranging from possible warming outcomes of 0.75-4.5 °K, with the most likely warming of about 2.5 °K. The HFDs also indicate that this region could see increases or decreases in precipitation (**Figure 11**), but that the chances are greater for increases with ~65% of the distribution’s population in both the no-policy and a “Level 2 Stabilization” (L2S, Webster *et al.*, 2010) scenarios. The HFD of the L2S scenario, which limits the equivalent CO₂ concentrations to ~650 ppm by the end of the century, indicates a 0.75 °K decrease in the most likely warming, compared to the no-policy scenario (**Figure 12**). Further, the shift in the HFD of the L2S scenario indicates that the

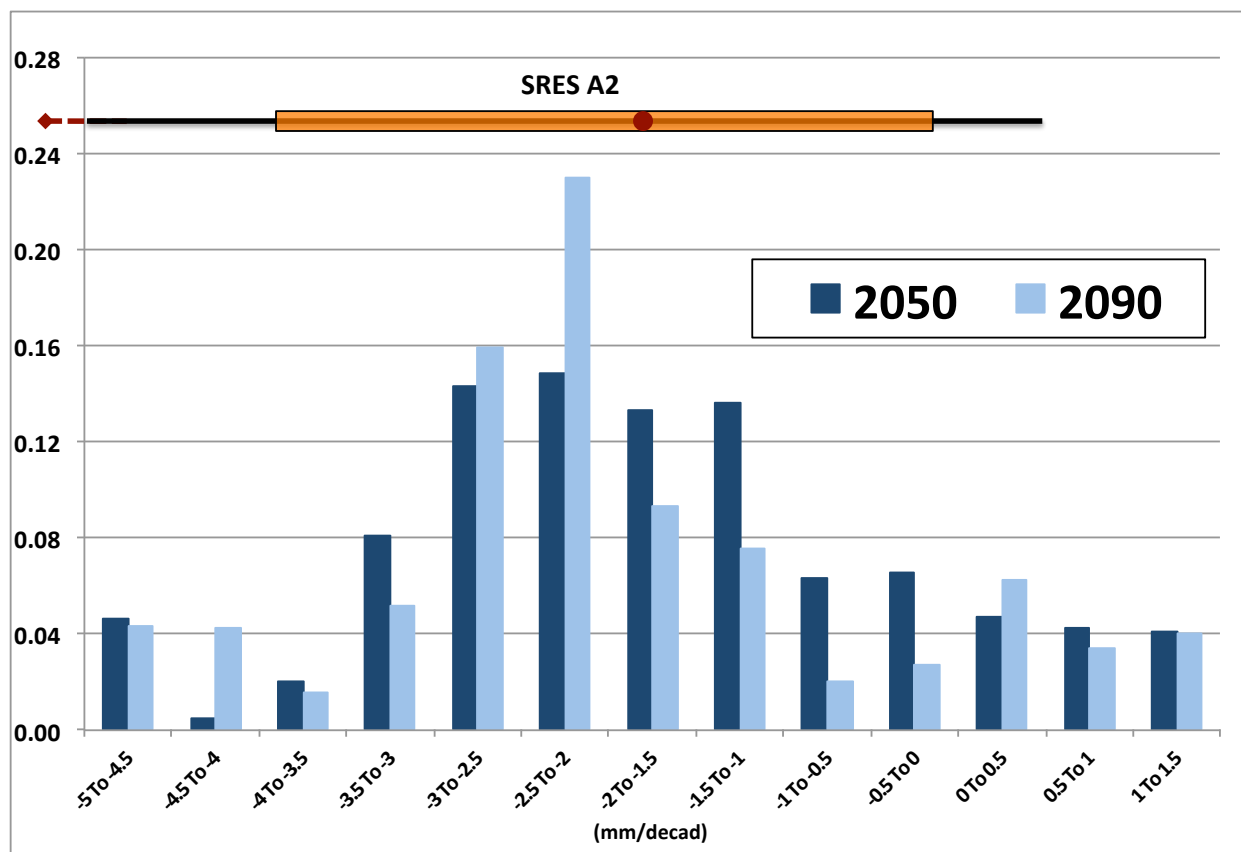


Figure 14. Hybrid frequency distributions (HFDs) of decadal averaged June-August (JJA) precipitation change (with respect to the last decade of the 20th century). The changes are area averaged for the Europe (EURP) region (boxed region denoted in Figures 3-7). Shown are the decadal averaged results starting at 2050 (dark blue bars) and 2090 (light blue bars), based on the no-policy IGSM ensemble simulation. Also denoted by the whisker plot are climate-model decadal JJA precipitation changes at 2050 from the A2 scenario of the IPCC AR4. The red circle indicates the median, the boxed region indicates the inter-quartile range, and the black line spans the minimum and maximum change. In this case, the minimum value (-7.8 mm/decad) extends beyond the abscissa range and is denoted by the dashed red line. This minimum value represents the only AR4 climate model that falls outside the HFD population.

chances of the warmest outcomes in the no-policy scenario are removed. Similarly, the L2S scenario HFD results in shifts of the distribution's population toward weaker precipitation increases, as seen most noticeably by a removal of any chance of the most extreme precipitation increases (**Figure 13**). The L2S scenario also results in a 27% increases in the frequency of the weakest precipitation changes.

3.2 Western Europe (EURP) Region

According to the IPCC AR4 results (IPCC, 2007), climate models convey a consensus of strong decreases in precipitation over much of Europe during the summer months (June-August)

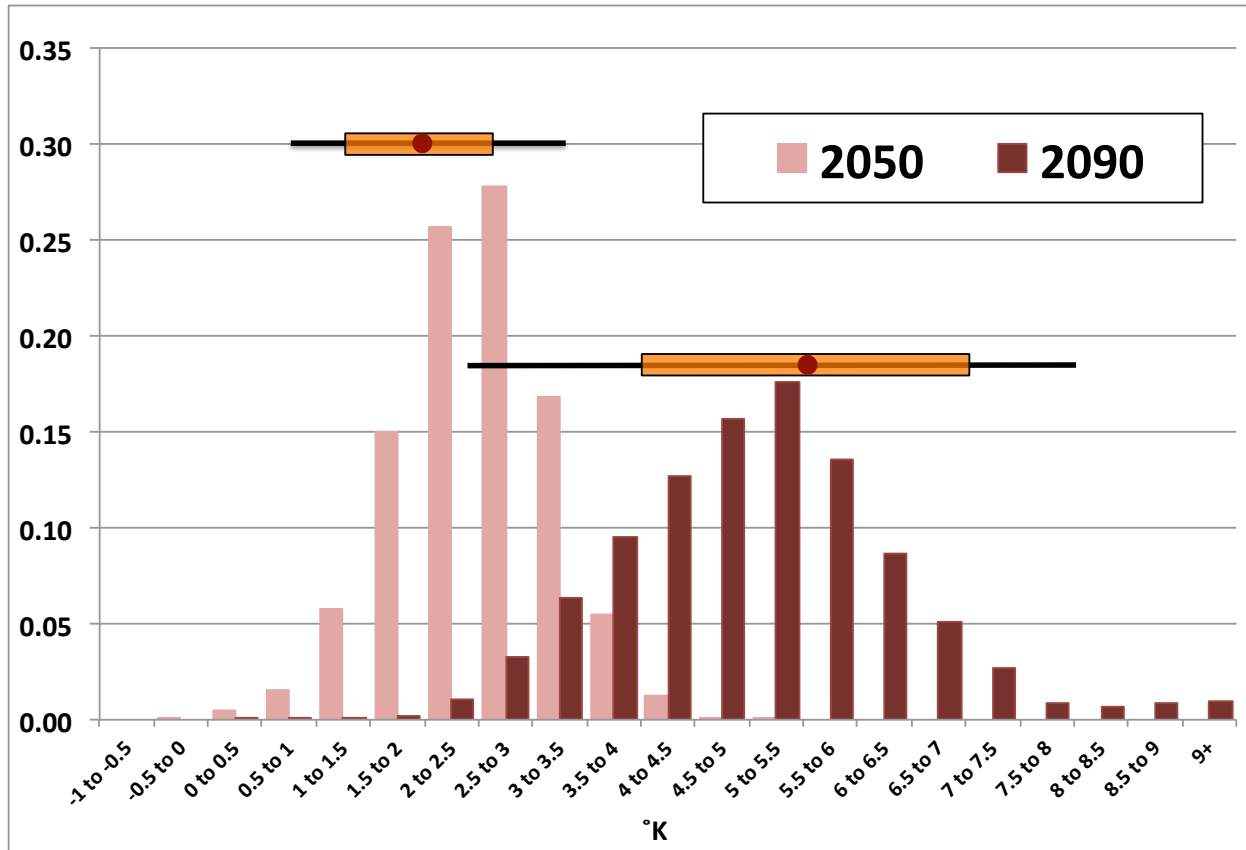


Figure 15. Hybrid frequency distributions (HFDs) of decadal averaged June-August (JJA) surface-air temperature (T_a) change (with respect to the last decade of the 20th century). The changes are area averaged for the Europe (EURP) region (boxed region denoted in Figures 3-7). Shown are the results starting at 2050 (light red bars) and 2090 (dark red bars), based on the no-policy IGSM ensemble simulation. Also denoted in the figure by the whisker plots are summaries of the corresponding climate-model decadal JJA changes at 2050 from the A2 scenario of the IPCC AR4. The red circle indicates the median, the boxed region indicates the inter-quartile range, and the black line spans the minimum and maximum change.

in response to human-induced warming. The median of this IPCC climate-model consensus is also conveyed by the no-policy HFD (Figure 14, 2050 conditions are compared). Exact consistency between the A2 collective and HFD is not expected, since the A2 scenario represents only one possible concentration scenario against the many possible emission “no-policy” pathways as well as climate parameter and regional downscale combinations of the IGSM represented by these HFDs. Nevertheless, the bulk of the HFD population qualitatively aligns with the inter-quartile range of the 19 climate models’ A2 result. Some notable differences are that the 10% of the HFD population contains precipitation changes (at 2050) higher than the A2 result and that one of the A2 climate models (GFDL) shows a much stronger decrease in precipitation than any of the HFD members. By the end of the century, the HFD indicates a slight convergence of its population, resulting in a more salient mode of precipitation change in

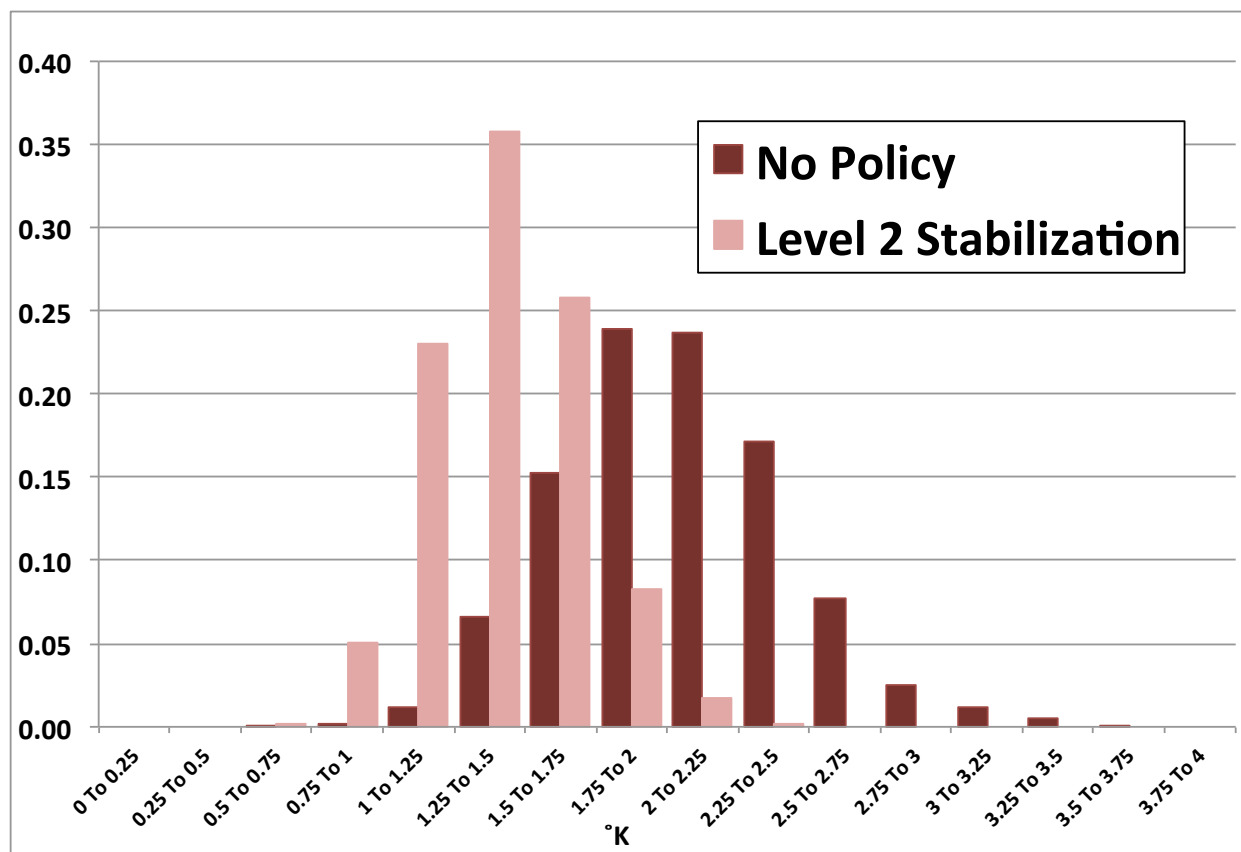


Figure 16. Hybrid frequency distributions (HFDs) of decadal averaged surface-air temperature (T_a) change (with respect to the last decade of the 20th century). The changes are area averaged for the Blue Nile (BLNL) region (boxed region denoted in Figures 3-7). Shown are the decadal averaged results starting at 2050, based on the no-policy IGSM ensemble simulation (dark red bars) and the Level 2 stabilization scenario (light red bars).

the range of -2.5 to -2.0 mm/decad. This clustering of decreased precipitation is also qualitatively consistent with the A2 results (not shown), however their clustering occurs at a lower value (~ 3.5 mm/decad) and could be a result of the single A2 concentration pathway and/or limited parametric and model sample. A quantitative diagnoses of the cause of these expected differences lies beyond the scope of this presentation. Nevertheless, under a similar diagnosis, we find that the results of the HFD analysis provide a depiction of the changes in global T_a that aligns with the IPCC AR4 results (**Figure 15**). The salient features of the HFD distributions are the occurrences of both smaller and larger increases in temperature with respect to the AR4 range, which would be expected (but not necessarily assured) given larger sample size of the HFD ensemble population. A very small fraction of the distribution ($\sim 1\%$) indicates temperature changes in excess of 9 °K by 2090. Conversely, less than 1% of the ensemble population indicates a warming of less than 1 °K to occur by the end of the century.

3.3 Blue Nile Region (BLNL)

The Blue Nile region represents one of the most contentiously managed water basins of the world, with multi-national upstream/downstream interests to harvest its water supply. Changes in air temperature can dramatically affect potential evaporation rates and thus the depletion of

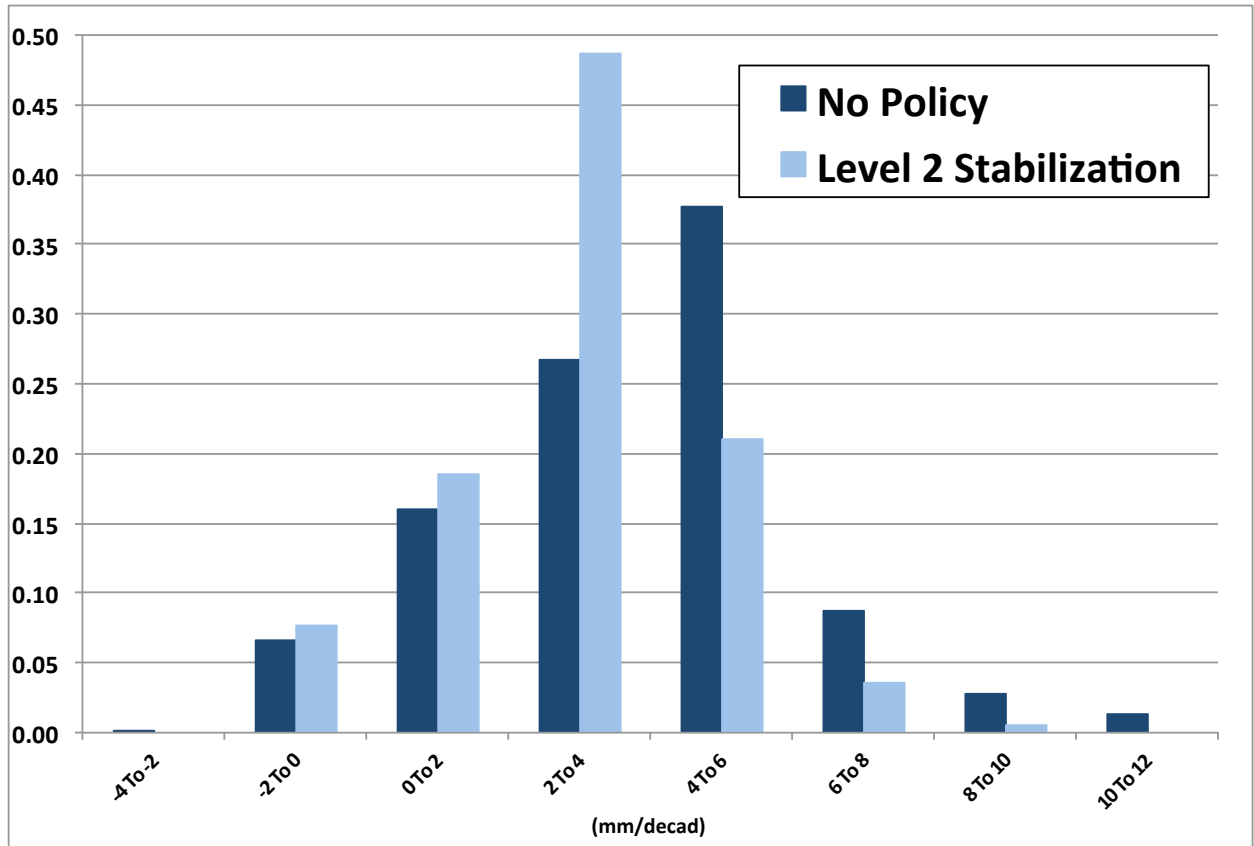


Figure 17. Hybrid frequency distributions (HFDs) of decadal averaged precipitation change (with respect to the last decade of the 20th century). The changes are area averaged for the Blue Nile (BLNL) region (boxed region denoted in Figures 3-7). Shown are the decadal averaged results starting at 2050, based on the no-policy IGSM ensemble simulation (dark blue bars) and the Level 2 stabilization scenario (light blue bars).

reservoirs, particularly the shallow reservoirs which cover a large surface area (such as the Aswan), and further shifts and changes in precipitation can buffer or exacerbate these conditions. The HFD results indicate that most likely this region would experience a ~ 2 °K warming by 2050 in the absence of any climate policy, and all of the HFD population indicate a warming of at least 0.75 °K with a maximum warming of as high as 3.75 °K (**Figure 16**). Under the L2S scenario, the mode of the HFD reduces to a 1.25-1.5 °K, and similar to the SWUS results, all but 3% of the entire population resides in the lower half of the no-policy HFD. Nevertheless, the stabilization

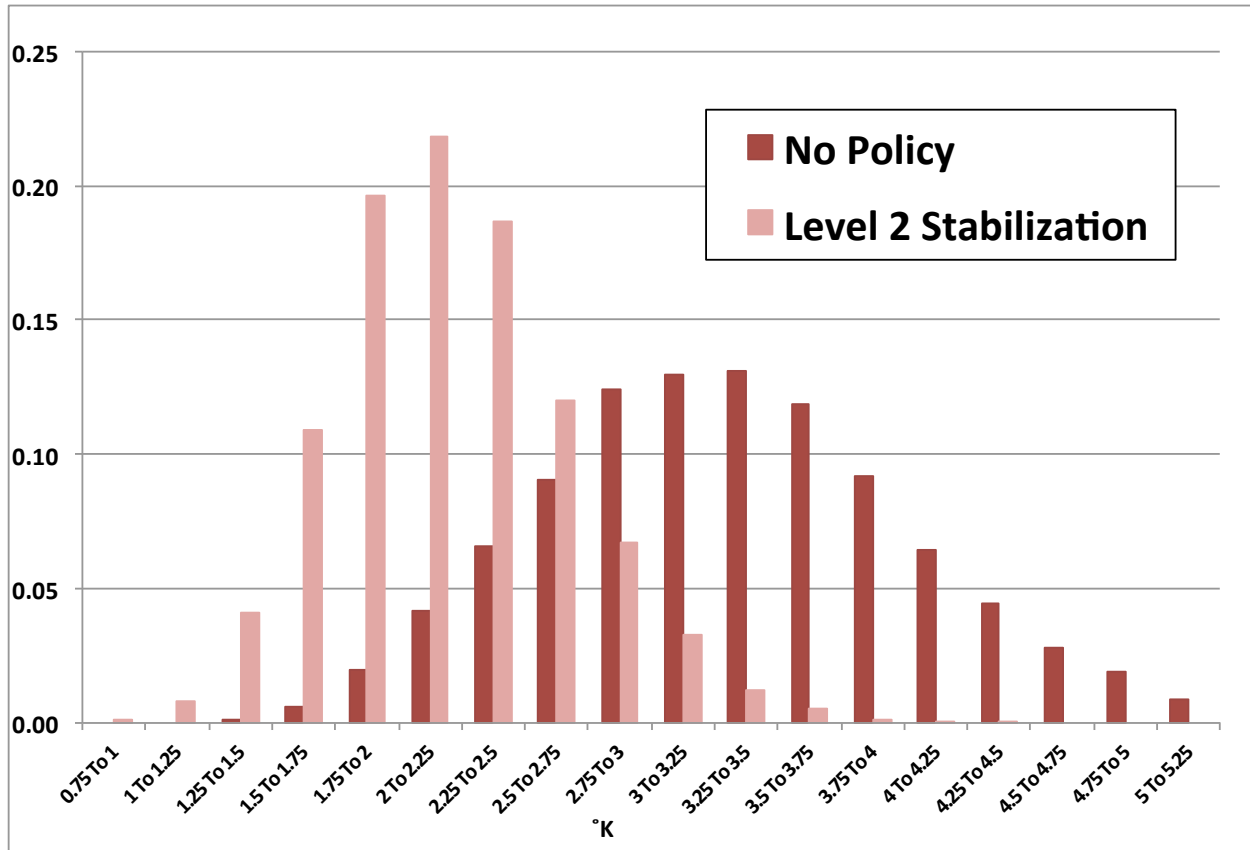


Figure 18. Hybrid frequency distributions (HFDs) of decadal averaged surface-air temperature (T_a) change (with respect to the last decade of the 20th century). The changes are area averaged for the yedoma (YDMA) region (boxed region denoted in Figures 3-7). Shown are the decadal averaged results starting at 2050, based on the no-policy IGSM ensemble simulation (dark red bars) and the Level 2 stabilization scenario (light red bars).

scenario has little effect on the minimum warming, which remains at 0.75 °K. The L2S scenario has somewhat more subtle effects on the precipitation HFD (**Figure 17**). The notable shift in the mode of precipitation change indicates that the most likely increase would not be as large under climate policy. However, both scenarios show that 6-7 % of the HFD population shows decreased precipitation over the region, and that this occurrence is not very responsive to policy. Across the higher end of the precipitation change distributions, climate policy does lead to decreases in the population bins, but only in the largest increase of precipitation does the L2S policy completely remove any chance of occurrence.

3.4 Yedoma Region (YDMA)

Much of the soil landscape of the northernmost region of Siberia is characterized as yedoma, which signifies the carbon-rich content of the soil that extends 100's of meter deep (Walter *et al.*, 2006). Until recently, the soil in this region has also been locked up in a permafrost state, but recent warming over the past century and the continued warming of this region threatens a

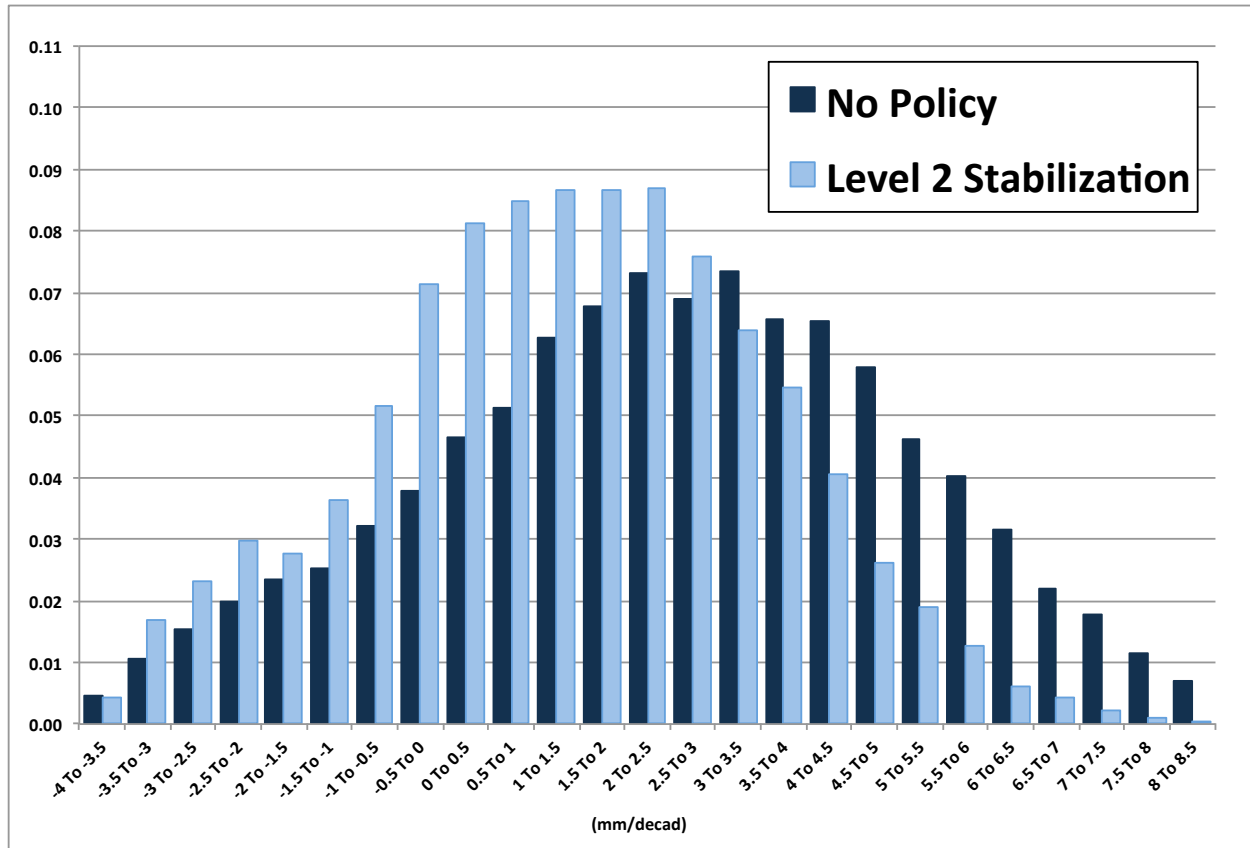


Figure 19. Hybrid frequency distributions (HFDs) of decadal averaged precipitation change (with respect to the last decade of the 20th century). The changes are area averaged for the Amazon (AMZN) region (boxed region denoted in Figures 3-7). Shown are the decadal averaged results starting at 2050, based on the no-policy IGSM ensemble simulation (dark blue bars) and the Level 2 stabilization scenario (light blue bars).

widespread thawing and subsequent adverse consequences to infrastructure, such as gas pipelines (e.g. Paltsev, 2011) and potentially strong biogeochemical feedbacks to the climate system (Zhuang *et al.*, 2006). We focus our HFD analysis on a core area of the yedoma region (denoted by the YDMA box in Figures 3-7), where some of the coldest conditions and richest soils exist (Walter *et al.*, 2006). By the middle of this century, the HFD results indicate that the most likely warming will be in the range of 3.25-3.5 °K, and that 50% of the HFD population lies above this warming (**Figure 18**). At this warming rate, half of the total permafrost area of the pan-arctic region will have thawed (e.g. Lawrence and Slater, 2007), with nearly complete degradation by the end of the 21st century. The largest warming that this region could experience (by 2050) is in the range of 5.0-5.25 °K. Under a moderate climate policy, nearly all of the HFD population lies below this degradation situation. Moreover, the mode of the distribution has decreased by 1 °K.

3.5 Amazon Region (AMZN)

With its rich biodiversity, ubiquitous rainforest conditions, and the largest outflow of freshwater into the world’s oceans, the Amazon River basin is among the most influential watersheds of the global environment. Changes to this environment whether a direct consequence of human activities (i.e. deforestation) or a result of a global climate shift are of paramount importance. One striking aspect of the HFD of precipitation (**Figure 19**) for this region is the large spread of change for the region, which positive and negative. Overall, the positive changes reach a higher magnitude (about doubled) than the negative among the HFD population, and the mode of the distribution lies in positive precipitation change (~3.0 mm/decad). The effect of policy is subtle, but causes a notable shift in the skewness of the distribution with the population of the highest precipitation increases diminished. This, in turn, causes the mode value of precipitation increase to diminish to ~1.5 mm/decad, but the peak of the distribution is broad and ranges from 1.0-2.5 mm/decad. The occurrence of decreases in

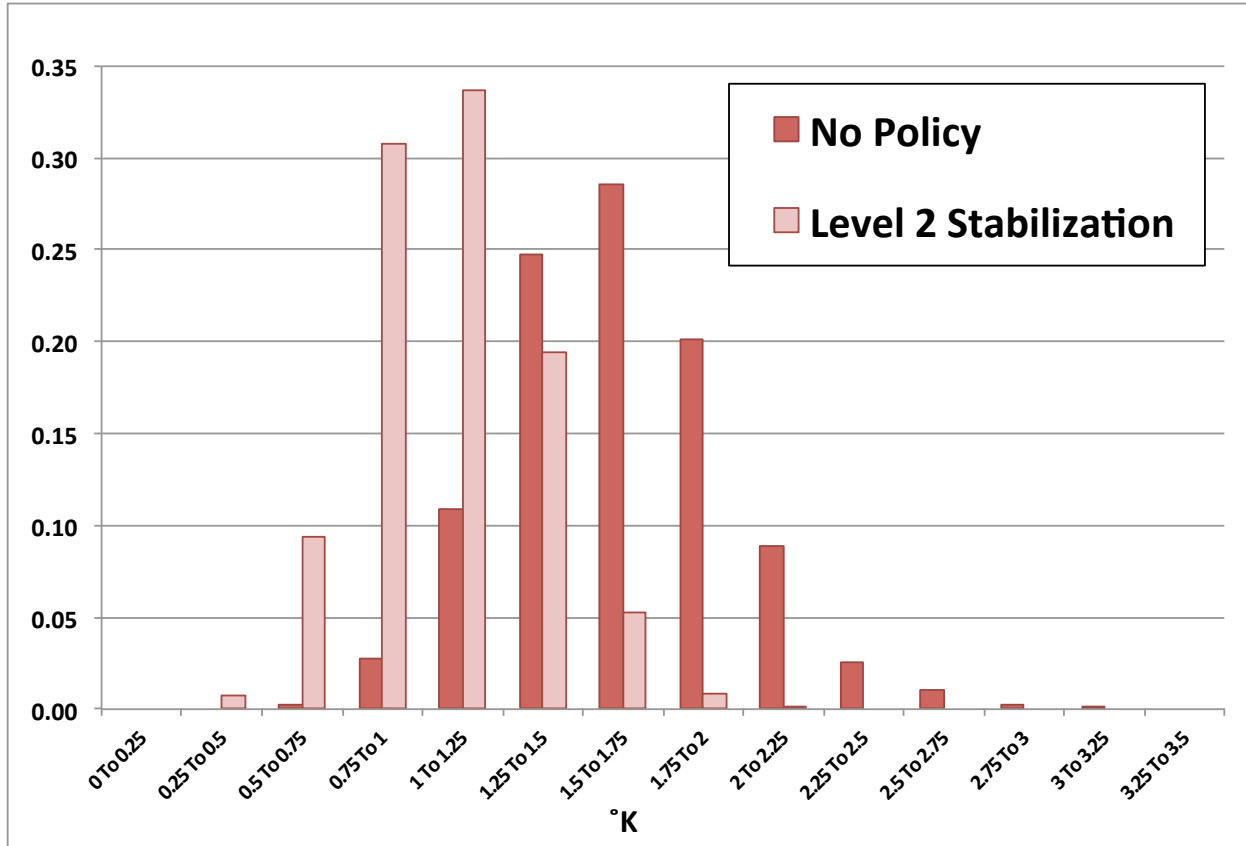


Figure 20. Hybrid frequency distributions (HFDs) of decadal averaged surface-air temperature (T_a) change (with respect to the last decade of the 20th century). The changes are area averaged for the southeastern Australia (SEAU) region (boxed region denoted in Figures 3-7). Shown are the decadal averaged results starting at 2050, based on the no-policy IGSM ensemble simulation (dark red bars) and the Level 2 stabilization scenario (light red bars).

precipitation is slightly enhanced, but they are not as extensive as seen in the precipitation increases.

3.6 Southeastern Australia Region (SEAU)

Australia can be characterized, geographically speaking, as being dominated by harsh, arid conditions in its interior, continental regions. One region in contrast to this is the southeastern region (Figures 3-7) with its relatively cooler conditions (Figure 1), higher rates of precipitation (Figure 2) throughout most of the year, as well as containing a substantial portion of the country’s population. By the middle of the 21st century, and in the absence of any stabilization policy, the central tendency of the IGSM HFD indicates a 1.5-1.75 °K warming, and nearly 75%

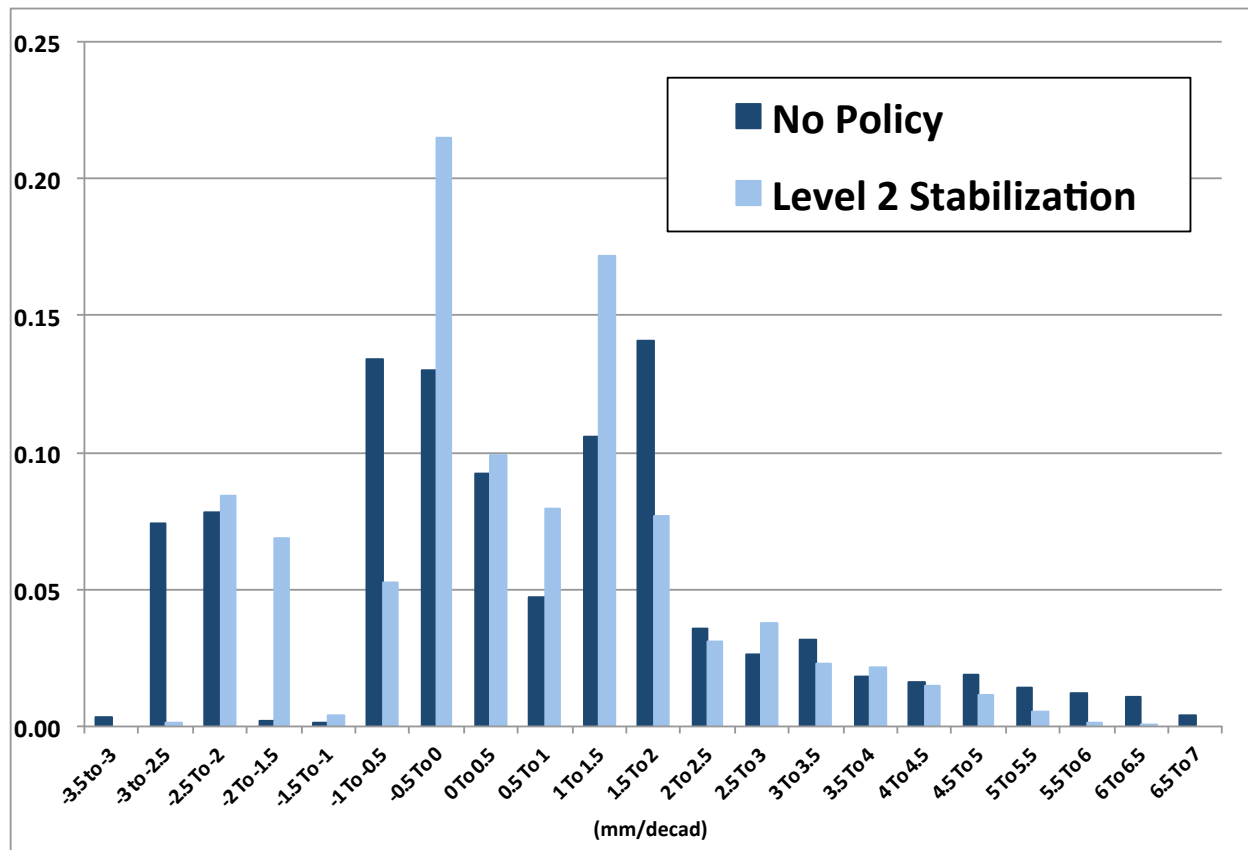


Figure 21. Hybrid frequency distributions (HFDs) of decadal averaged precipitation change (with respect to the last decade of the 20th century). The changes are area averaged for the southeastern Australia (SEAU) region (boxed region denoted in Figures 3-7). Shown are the decadal averaged results starting at 2050, based on the no-policy IGSM ensemble simulation (dark blue bars) and the Level 2 stabilization scenario (light blue bars).

of the distribution lies within the range of 1.25-2.0 °K (**Figure 20**). About 3% of the distribution results in the warming of less than 1 °K, and less than 1% of the meta-ensemble’s population indicates a warming of greater than 3 °K. Through the Level 2 Stabilization scenario, the central tendency of warming declines by 0.5 °K (or a 33% reduction), and the fraction of the ensemble

population that immediately flanks the mode increases. Under policy, the skewness of the HFD is affected somewhat such that a slightly smaller portion of the model population lies above the mode value of warming (32% for no policy compared to 25% for the Level 2 Stabilization).

For precipitation (**Figure 21**) the structure of the HFDs between the no policy and Level 2 Stabilization scenarios are more skewed and less cohesive than that of temperature. For the no policy HFD, the model population shows that, generally speaking, both increases and decreases of precipitation could be seen over the region, and as such, the shape of the distribution is bimodal. However, the HFDs are able to characterize the probabilistic nature of these decreases

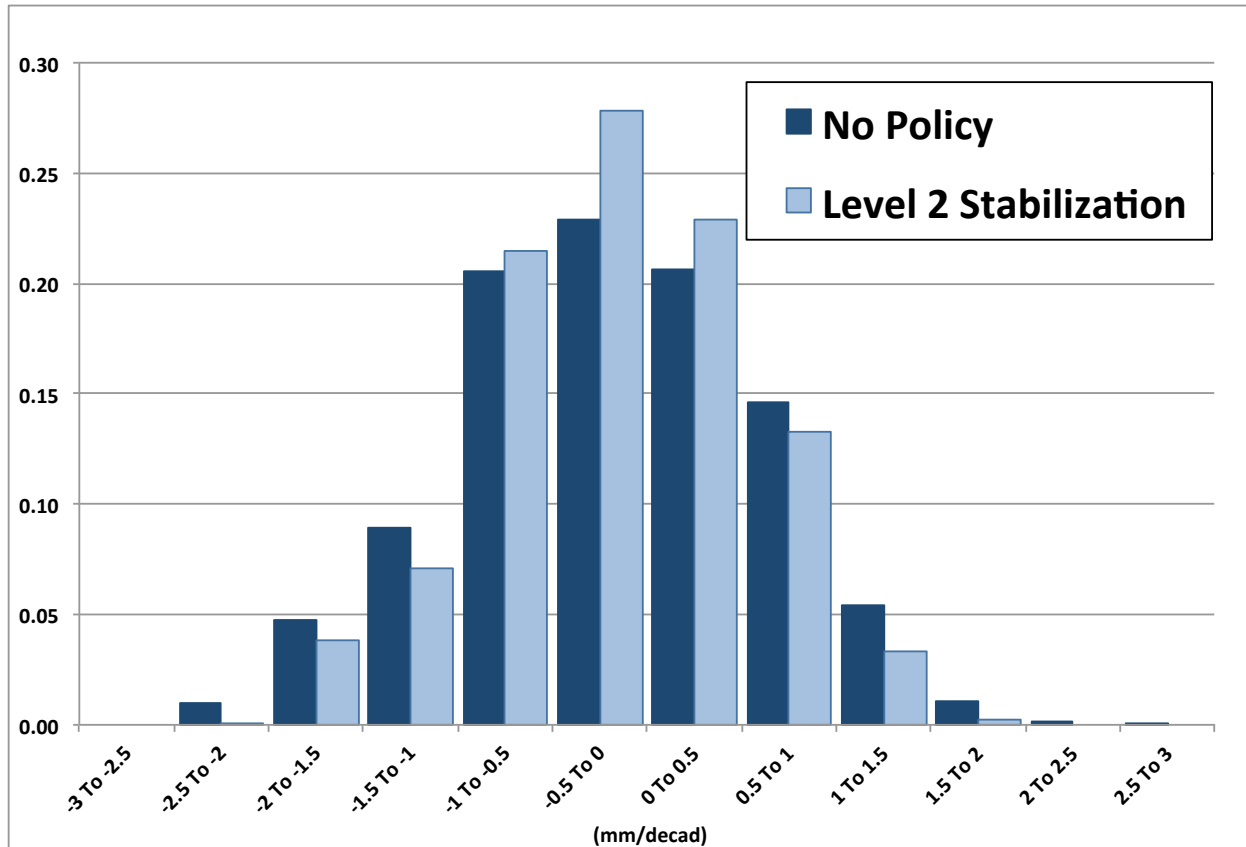


Figure 22. Hybrid frequency distributions (HFDs) of decadal averaged precipitation change (with respect to the last decade of the 20th century). The changes are area averaged for the South Africa (SAFR) region (boxed region denoted in Figures 3-7). Shown are the decadal averaged results starting at 2050, based on the no-policy IGSM ensemble simulation (dark blue bars) and the Level 2 stabilization scenario (light blue bars).

and increases quite differently. The increases in precipitation exhibit a much more pronounced tail in the distribution, and indicate slight occurrences (1-2 % of the model population for each bin) double in magnitude to any of the decreases. The distribution of decreased precipitation exhibits more of a clustered behavior, with distinct occurrences of values in the range of -3.0 to -2.0 mm/decad. The largest fraction of the model population occurs in the -1.0 to -0.5 mm/decad range. Notwithstanding these distinctly different features between positive and negative regions

of the distribution, the HFD is only slightly skewed with respect to the sign of precipitation change, with 42% of the population showing decreases and 58% of the population with increases. Under climate policy, occurrences of the highest changes are buffered (or removed) and shifted toward lower values. With these shifts, the minimum and maximum values of the precipitation-change distribution decrease by about 15%. This also results in a more pronounced bimodality about the median of the distribution, and in particular, the decrease precipitation feature becomes more salient compared to its increase counterpart.

3.6 South Africa Region (SAFR)

According to the IPCC AR4 results (IPCC, 2007), a substantial fraction of the climate models indicate widespread decreases in precipitation. Yet in studies using regional methods, the results are mixed with both decreases and increases in precipitation projected under human-forced change (Thomas *et al.*, 2007). The HFDs of the IGSM meta-ensemble indicate a mixed situation for precipitation changes (**Figure 22**), with a nearly equal distribution of both increases and decreases in precipitation with 42% versus 58%, respectively, for the No Policy case (thus a slightly greater chance for decreased precipitation). Further, there is a slight skewness to the distribution in that a small number of the population members achieve increased precipitation values that exceed, in magnitude, any decreases in precipitation. The impact of policy is subtle, but the most notable effect on the HFD is seen in the reduction of the occurrence the most extreme changes, and in particular, the largest change in precipitation increase seen in the distribution is reduced by 33% (from 3 mm/decad to 2 mm/decad). These reductions in the occurrence of the largest changes then directly contribute to a more pronounced mode in the HFD, but the location of the mode (a small decrease) is unchanged.

4. CLOSING REMARKS

We have presented a technique that transforms the zonal information of the IGSM on climate-variable trends into longitudinal detail. This is achieved through a linear (Taylor) expansion of the changes in the longitudinal patterns (normalized by its respective zonal mean) as a function of global temperature change. These pattern shifts are derived from model results from the IPCC AR4 SRES scenarios, and then normalized with respect to their climate sensitivity. We have constructed monthly climatologies of these climate-change patterns from the AR4 archive and have found that for any given climate model these derived pattern changes are robust across all of the SRES scenarios considered. With the entire AR4 model collective, we can combine each of these climate-change pattern transformations to all of the ensemble-simulation members of the IGSM that have been produced for climate-policy analysis, which then enhances the spatial details of the IGSM. Combined, these augmented simulations form the basis for “hybrid frequency distributions” (HFDs) for any particular region of interest. Our presented analyses focused on applying this technique to surface-air temperature and precipitation. However, this technique could, in principle, be applied to any variable of interest.

Given these meta-ensembles, we construct surface-air temperature and precipitation HFDs for a number of selected regions across the global to assess their features as well as the shifts due to

climate policy (or lack thereof). In a comparison of “no policy” climate-change projections, the corresponding HFD of the IGSM was found to have comparable characteristics, especially for surface-air temperature, to the (albeit limited) sample of the AR4 models. The HFDs from no-policy and greenhouse-gas stabilization IGSM projections were then examined for a selection of regions across the globe. Among all the regions considered, we find that the HFDs are able to produce salient features in the distributions that characterize and quantify the effect of climate policy on reducing the odds of warming – seen in both as a shift in the mode of the HFD as well as the removal of the most extreme warming outcomes. In most cases, the minimum warming in the HFD is largely unaffected. For precipitation, the HFDs paint a more complex picture, in most cases showing chances of increases and decreases by the middle of this century. The effect of policy, generally speaking, is to constrict the total range of possible outcomes in the distribution. In terms of modal shifts, we find mixed results among the regions considered. Some regions show very small changes between climate policies, while others show notable buffering from the greenhouse-gas stabilization target.

Recent studies with the IPCC AR4 archive have focused on the apparent need to filter and/or weight or filter certain climate model according to a chosen skill metric (e.g. Shukla *et al.*, 2006) and the general aspects that filtering has on resulting analyses (e.g., Weigel *et al.*, 2010). Some of these efforts were motivated either by computational constraints of vetting the data through impact models or for the purpose of highlighting the more “reliable” results and implying that these modeled outcomes were, in a sense, “more likely”. More recent model analyses have emphasized that caution must be taken in the interpretation of model skill in this regard (e.g. Knutti *et al.*, 2010; Reifen and Toumi, 2009). Any filtering in this regard will undoubtedly be a complex function of: the variables of interest, their use, their temporal frequency, the region/domain of focus, the skill/filtering metric(s) chosen, time period of interest, and the climate events and/or phenomenon that are of particular concern as well as the important spatio-temporal scales in this regard. Given these issues, this study makes no deliberate attempt to filter out any modeled outcomes and, as such, considers all members of the HFD meta-ensemble equally. Recent analyses support equal weighting as robust, particularly in the absence of any comprehensive, quantitative description of climate-model performance (e.g. Weigel *et al.*, 2010 and DelSole *et al.*, 2011). Nevertheless, our ongoing efforts are exploring the use of Gaussian quadrature techniques (e.g. Arndt *et al.*, 2006) to limit the meta-ensemble size, while preserving the statistical moments of key parameters, prior to its application in impact and/or adaptation assessments. The downsized ensemble would therefore reduce computational demand, while preserving the scope and character of the resulting impact/risk assessment.

Notwithstanding these issues, to quantify the true climate risk and societal implications of these HFDs, the transformed IGSM variables require further vetting through impact assessment models. These presented variables, as well as other atmospheric variables of interest, can be produced for any domain of interest for an appropriate climate-scale grid (e.g. 2°x2°). Our downscaling efforts with the IGSM are ongoing and a future paper will assess the feasibility of employing higher-resolution regional climate model projections – such as those from the recent

North American Regional Climate Change Assessment Project (NARCCAP, Mearns *et al.*, 2009), to provide these HFDs at even greater regional and spatial detail.

Acknowledgments

This work was funded by the U.S. Department of Energy's Abrupt Climate Change program, grant # DE-FG02-08ER64597. The authors also gratefully acknowledge additional financial support for this work provided by the MIT Joint Program on the Science and Policy of Global Change through a consortium of industrial sponsors and Federal grants. Development of the IGSM applied in this research was supported by the U.S. Department of Energy, Office of Science (DE-FG02-94ER61937); the U.S. Environmental Protection Agency, EPRI, and other U.S. government agencies and a consortium of 40 industrial and foundation sponsors. For a complete list see <http://globalchange.mit.edu/sponsors/current.html>. The authors would also like to thank Henry Jacoby for his valuable discussions and editorial remarks in earlier versions of this manuscript.

REFERENCES

- Arndt, C., J. Kozlitina, and P. V. Preckel, 2006: Efficient survey sampling of households via Gaussian quadrature. *J. Royal Stat. Soc.: Series C (Applied Statistics)*, **55**, 355–364. doi: 10.1111/j.1467-9876.2006.00537.
- Broccoli, A. J., N.-C. Lau, and M. J. Nath, 1998: The cold ocean–warm land pattern: Model simulation and relevance to climate change detection. *J. Climate*, **11**, 2743–2763.
- Climsystem, 2011, <http://www.climsystems.com/>
- DelSole, T., X. Yang, and M. K. Tippett, 2011: Is Unequal Weighting Significantly Better than Equal Weighting for Multi-Model Forecasting? *J. Climate*, submitted.
- EPRI, 2005: COuntry Specific Model for Intertemporal Climate (COSMIC 2), Electric Power Research Institute.
- Furrer, R., R. Knutti, S.R. Sain, D.W. Nychka, and G. A. Meehl, 2007: Spatial patterns of probabilistic temperature change projections from a multivariate Bayesian analysis. *Geophys. Res. Letters*, **34**, L06711, DOI:10.1029/2006GL027754.
- Hulme, M., S.C. Raper, and T. Wigley, 1995: An Integrated Framework to Address Climate Change (ESCAPE) and Further Developments of the Global and Regional Climate Modules (MAGICC), *Energy Policy*, **23**, 347-355.
- Jones, P.D., New, M., Parker, D.E., Martin, S. and Rigor, I.G., 1999: Surface air temperature and its variations over the last 150 years. *Reviews of Geophysics* **37**, 173-199.
- Knutti, R., 2010: The end of model democracy?, *Climatic Change*, **102**, 395-404, doi 10.1007/s10584-010-9800-2.
- Knutti, R., R. Furrer, C. Tebaldi, J. Cermak, G. Meehl, 2010: Challenges in combining projections from multiple climate models. *J. Climate*, **23**, 2739–2758.
- Mearns, L. O., W. J. Gutowski, R. Jones, L.-Y. Leung, S. McGinnis, A. M. B. Nunes, and Y. Qian, 2009: A regional climate change assessment program for North America. *EOS*, **90**, 36, 311-312.
- Paltsev S., J. Reilly, H. Jacoby, R. Eckaus, J. McFarland, M. Sarofim, M. Asadoorian and M. Babiker, 2005: The MIT Emissions Prediction and Policy Analysis (EPPA) Model:

Version 4. MIT Joint Program Report 125

(http://globalchange.mit.edu/files/document/MITJPSPGC_Rpt125.pdf).

- Paltsev, S., 2011: Russia's Natural Gas Export Potential up to 2050, MIT Joint Program Report 201, http://globalchange.mit.edu/files/document/MITJPSPGC_Report_201.pdf
- Reifen, C., and R. Toumi, 2009, Climate projections: Past performance no guarantee of future skill?, *Geophys. Res. Lett.*, **36**, doi:10.1029/2009GL038082.
- Santer, B. D., T. M. L. Wigley, M. E. Schlesinger, and J. F. B. Mitchell, 1990: Developing Climate Scenarios from Equilibrium GCM Results. Max-Planck-Institut für Meteorologie Report No. 47, Hamburg, Germany, 29 pp.
- Schlesinger, M.E., S. Malyshev, E.V. Rozanov, F. Yang, N.G. Andronova, B. de Vries, A. Grübler, K. Jiang, T. Masui, T. Morita, J. Penner, W. Pepper, A. Sankovski and Y. Zhang, 2000: Geographical distributions of temperature change for scenarios of greenhouse gas and sulfur dioxide emissions, *Tech. Forecast. Soc. Change*, **65**, 167-193.
- Schlesinger, M.E. and S. Malyshev, 2001 Changes in near-surface temperatures and sea level for the Post-SRES CO₂-stabilization scenarios, *Integrated Assessment*, **2**, 95-110.
- Schlesinger, M.E., S. Malyshev, E.V. Rozanov, F. Yang, N.G. Andronova, B. de Vries, A. Grübler, K. Jiang, T. Masui, T. Morita, J. Penner, W. Pepper, A. Sankovski and Y. Zhang, 2000: Geographical distributions of temperature change for scenarios of greenhouse gas and sulfur dioxide emissions, *Tech. Forecast. Soc. Change*, **65**, 167-193.
- Seager, R., and Coauthors, 2007: Model projections of an imminent transition to a more arid climate in southwestern North America. *Science*, **316**, 1181-1184.
- Shukla, J., T. DelSole, M. Fennessy, J. Kinter, and D. Paolino, 2006: Climate Model Fidelity and Projections of Climate Change. *Geophys. Res. Lett.*, **33**, L07702, doi:10.1029/2005GL025579.
- Sokolov, A. P., P. H. Stone, C. E. Forest, R. Prinn, M. C. Sarofim, M. Webster, S. Paltsev, C. A. Schlosser, D. Kicklighter, S. Dutkiewicz, J. Reilly, C. Wang, B. Felzer, H. D. Jacoby, 2009: Probabilistic forecast for 21st century climate based on uncertainties in emissions (without policy) and climate parameters, *J. Climate*, doi: 10.1175/2009JCLI2863.1.
- Thomas, D. S. G., C. Twyman, H. Osbahr, and B. Hewitson, 2007: Adaptation to climate change and variability: farmer responses to intra-seasonal precipitation trends in South Africa, *Climatic Change*, **83**, 301–322, doi: 10.1007/s10584-006-9205-4
- Warrick, R., 2009: From CLIMPACTS to SimCLIM: development of an integrated assessment model system, *Integrated Regional Assessment of Global Climate Change*. Eds: C. G. Knight, J. Jäger. *Cambridge University Press*, 280-311.
- Webster, M., A. P. Sokolov, J. M. Reilly, C. E. Forest, S. Paltsev, C. A. Schlosser, C. Wang, D. Kicklighter, M. Sarofim, J. Melillo, R. G. Prinn and H. D. Jacoby, 2011: Analysis of climate policy targets under uncertainty. *Climatic Change* (in press).
- Webster, M. D., C. E. Forest, J. M. Reilly, M. H. Babiker, D. W. Kicklighter, M. Mayer, R. G. Prinn, M. C. Sarofim, A. P. Sokolov, P. H. Stone and C. Wang, 2003. Uncertainty analysis of climate change and policy response. *Climatic Change*, **61**: 295-320; MIT Joint Program Reprint 2003-11; http://mit.edu/globalchange/www/MITJPSPGC_Reprint03-11.pdf.
- Wigley, T., 2011: <http://www.cgd.ucar.edu/cas/wigley/magicc/about.html>

- Williams, L. J., Shaw, D., Mendelsohn, R: 1998: Evaluating GCM Output with Impact Models, *Climatic Change*, **38**: 111-133.
- Yohe, G. and M. E. Schlesinger, 1998: Sea-Level Change: The Expected Economic Cost of Protection or Abandonment in the United States, *Climatic Change*, **39**: 337-472.
- Zhuang, Q., J. M. Melillo, M. C. Sarofim, D. W. Kicklighter, A. D. McGuire, B. S. Felzer, A. Sokolov, R. G. Prinn, P. A. Steudler and S. Hu, 2006: CO₂ and CH₄ exchanges between land ecosystems and the atmosphere in northern high latitudes over the 21st century. *Geophys. Res. Lett.* **33**, L17403, doi: 10.1029/2006GL026972.

REPORT SERIES of the MIT Joint Program on the Science and Policy of Global Change

1. **Uncertainty in Climate Change Policy Analysis**
Jacoby & Prinn December 1994
2. **Description and Validation of the MIT Version of the GISS 2D Model** *Sokolov & Stone* June 1995
3. **Responses of Primary Production and Carbon Storage to Changes in Climate and Atmospheric CO₂ Concentration** *Xiao et al.* October 1995
4. **Application of the Probabilistic Collocation Method for an Uncertainty Analysis** *Webster et al.* January 1996
5. **World Energy Consumption and CO₂ Emissions: 1950-2050** *Schmalensee et al.* April 1996
6. **The MIT Emission Prediction and Policy Analysis (EPPA) Model** *Yang et al.* May 1996 (*superseded* by No. 125)
7. **Integrated Global System Model for Climate Policy Analysis** *Prinn et al.* June 1996 (*superseded* by No. 124)
8. **Relative Roles of Changes in CO₂ and Climate to Equilibrium Responses of Net Primary Production and Carbon Storage** *Xiao et al.* June 1996
9. **CO₂ Emissions Limits: Economic Adjustments and the Distribution of Burdens** *Jacoby et al.* July 1997
10. **Modeling the Emissions of N₂O and CH₄ from the Terrestrial Biosphere to the Atmosphere** *Liu* Aug. 1996
11. **Global Warming Projections: Sensitivity to Deep Ocean Mixing** *Sokolov & Stone* September 1996
12. **Net Primary Production of Ecosystems in China and its Equilibrium Responses to Climate Changes**
Xiao et al. November 1996
13. **Greenhouse Policy Architectures and Institutions**
Schmalensee November 1996
14. **What Does Stabilizing Greenhouse Gas Concentrations Mean?** *Jacoby et al.* November 1996
15. **Economic Assessment of CO₂ Capture and Disposal**
Eckaus et al. December 1996
16. **What Drives Deforestation in the Brazilian Amazon?**
Pfaff December 1996
17. **A Flexible Climate Model For Use In Integrated Assessments** *Sokolov & Stone* March 1997
18. **Transient Climate Change and Potential Croplands of the World in the 21st Century** *Xiao et al.* May 1997
19. **Joint Implementation: Lessons from Title IV's Voluntary Compliance Programs** *Atkeson* June 1997
20. **Parameterization of Urban Subgrid Scale Processes in Global Atm. Chemistry Models** *Calbo et al.* July 1997
21. **Needed: A Realistic Strategy for Global Warming**
Jacoby, Prinn & Schmalensee August 1997
22. **Same Science, Differing Policies; The Saga of Global Climate Change** *Skolnikoff* August 1997
23. **Uncertainty in the Oceanic Heat and Carbon Uptake and their Impact on Climate Projections**
Sokolov et al. September 1997
24. **A Global Interactive Chemistry and Climate Model**
Wang, Prinn & Sokolov September 1997
25. **Interactions Among Emissions, Atmospheric Chemistry & Climate Change** *Wang & Prinn* Sept. 1997
26. **Necessary Conditions for Stabilization Agreements**
Yang & Jacoby October 1997
27. **Annex I Differentiation Proposals: Implications for Welfare, Equity and Policy** *Reiner & Jacoby* Oct. 1997
28. **Transient Climate Change and Net Ecosystem Production of the Terrestrial Biosphere**
Xiao et al. November 1997
29. **Analysis of CO₂ Emissions from Fossil Fuel in Korea: 1961-1994** *Choi* November 1997
30. **Uncertainty in Future Carbon Emissions: A Preliminary Exploration** *Webster* November 1997
31. **Beyond Emissions Paths: Rethinking the Climate Impacts of Emissions Protocols** *Webster & Reiner* November 1997
32. **Kyoto's Unfinished Business** *Jacoby et al.* June 1998
33. **Economic Development and the Structure of the Demand for Commercial Energy** *Judson et al.* April 1998
34. **Combined Effects of Anthropogenic Emissions and Resultant Climatic Changes on Atmospheric OH** *Wang & Prinn* April 1998
35. **Impact of Emissions, Chemistry, and Climate on Atmospheric Carbon Monoxide** *Wang & Prinn* April 1998
36. **Integrated Global System Model for Climate Policy Assessment: Feedbacks and Sensitivity Studies**
Prinn et al. June 1998
37. **Quantifying the Uncertainty in Climate Predictions**
Webster & Sokolov July 1998
38. **Sequential Climate Decisions Under Uncertainty: An Integrated Framework** *Valverde et al.* September 1998
39. **Uncertainty in Atmospheric CO₂ (Ocean Carbon Cycle Model Analysis)** *Holian* Oct. 1998 (*superseded* by No. 80)
40. **Analysis of Post-Kyoto CO₂ Emissions Trading Using Marginal Abatement Curves** *Ellerman & Decaux* Oct. 1998
41. **The Effects on Developing Countries of the Kyoto Protocol and CO₂ Emissions Trading**
Ellerman et al. November 1998
42. **Obstacles to Global CO₂ Trading: A Familiar Problem**
Ellerman November 1998
43. **The Uses and Misuses of Technology Development as a Component of Climate Policy** *Jacoby* November 1998
44. **Primary Aluminum Production: Climate Policy, Emissions and Costs** *Harnisch et al.* December 1998
45. **Multi-Gas Assessment of the Kyoto Protocol**
Reilly et al. January 1999
46. **From Science to Policy: The Science-Related Politics of Climate Change Policy in the U.S.** *Skolnikoff* January 1999
47. **Constraining Uncertainties in Climate Models Using Climate Change Detection Techniques**
Forest et al. April 1999
48. **Adjusting to Policy Expectations in Climate Change Modeling** *Shackley et al.* May 1999
49. **Toward a Useful Architecture for Climate Change Negotiations** *Jacoby et al.* May 1999
50. **A Study of the Effects of Natural Fertility, Weather and Productive Inputs in Chinese Agriculture**
Eckaus & Tso July 1999
51. **Japanese Nuclear Power and the Kyoto Agreement**
Babiker, Reilly & Ellerman August 1999
52. **Interactive Chemistry and Climate Models in Global Change Studies** *Wang & Prinn* September 1999
53. **Developing Country Effects of Kyoto-Type Emissions Restrictions** *Babiker & Jacoby* October 1999

Contact the Joint Program Office to request a copy. The Report Series is distributed at no charge.

REPORT SERIES of the MIT Joint Program on the Science and Policy of Global Change

54. **Model Estimates of the Mass Balance of the Greenland and Antarctic Ice Sheets** *Bugnion* Oct 1999
55. **Changes in Sea-Level Associated with Modifications of Ice Sheets over 21st Century** *Bugnion* October 1999
56. **The Kyoto Protocol and Developing Countries** *Babiker et al.* October 1999
57. **Can EPA Regulate Greenhouse Gases Before the Senate Ratifies the Kyoto Protocol?** *Bugnion & Reiner* November 1999
58. **Multiple Gas Control Under the Kyoto Agreement** *Reilly, Mayer & Harnisch* March 2000
59. **Supplementarity: An Invitation for Monopsony?** *Ellerman & Sue Wing* April 2000
60. **A Coupled Atmosphere-Ocean Model of Intermediate Complexity** *Kamenkovich et al.* May 2000
61. **Effects of Differentiating Climate Policy by Sector: A U.S. Example** *Babiker et al.* May 2000
62. **Constraining Climate Model Properties Using Optimal Fingerprint Detection Methods** *Forest et al.* May 2000
63. **Linking Local Air Pollution to Global Chemistry and Climate** *Mayer et al.* June 2000
64. **The Effects of Changing Consumption Patterns on the Costs of Emission Restrictions** *Lahiri et al.* Aug 2000
65. **Rethinking the Kyoto Emissions Targets** *Babiker & Eckaus* August 2000
66. **Fair Trade and Harmonization of Climate Change Policies in Europe** *Viguier* September 2000
67. **The Curious Role of "Learning" in Climate Policy: Should We Wait for More Data?** *Webster* October 2000
68. **How to Think About Human Influence on Climate** *Forest, Stone & Jacoby* October 2000
69. **Tradable Permits for Greenhouse Gas Emissions: A primer with reference to Europe** *Ellerman* Nov 2000
70. **Carbon Emissions and The Kyoto Commitment in the European Union** *Viguier et al.* February 2001
71. **The MIT Emissions Prediction and Policy Analysis Model: Revisions, Sensitivities and Results** *Babiker et al.* February 2001 (*superseded* by No. 125)
72. **Cap and Trade Policies in the Presence of Monopoly and Distortionary Taxation** *Fullerton & Metcalf* March '01
73. **Uncertainty Analysis of Global Climate Change Projections** *Webster et al.* Mar. '01 (*superseded* by No. 95)
74. **The Welfare Costs of Hybrid Carbon Policies in the European Union** *Babiker et al.* June 2001
75. **Feedbacks Affecting the Response of the Thermohaline Circulation to Increasing CO₂** *Kamenkovich et al.* July 2001
76. **CO₂ Abatement by Multi-fueled Electric Utilities: An Analysis Based on Japanese Data** *Ellerman & Tsukada* July 2001
77. **Comparing Greenhouse Gases** *Reilly et al.* July 2001
78. **Quantifying Uncertainties in Climate System Properties using Recent Climate Observations** *Forest et al.* July 2001
79. **Uncertainty in Emissions Projections for Climate Models** *Webster et al.* August 2001
80. **Uncertainty in Atmospheric CO₂ Predictions from a Global Ocean Carbon Cycle Model** *Holian et al.* September 2001
81. **A Comparison of the Behavior of AO GCMs in Transient Climate Change Experiments** *Sokolov et al.* December 2001
82. **The Evolution of a Climate Regime: Kyoto to Marrakech** *Babiker, Jacoby & Reiner* February 2002
83. **The "Safety Valve" and Climate Policy** *Jacoby & Ellerman* February 2002
84. **A Modeling Study on the Climate Impacts of Black Carbon Aerosols** *Wang* March 2002
85. **Tax Distortions and Global Climate Policy** *Babiker et al.* May 2002
86. **Incentive-based Approaches for Mitigating Greenhouse Gas Emissions: Issues and Prospects for India** *Gupta* June 2002
87. **Deep-Ocean Heat Uptake in an Ocean GCM with Idealized Geometry** *Huang, Stone & Hill* September 2002
88. **The Deep-Ocean Heat Uptake in Transient Climate Change** *Huang et al.* September 2002
89. **Representing Energy Technologies in Top-down Economic Models using Bottom-up Information** *McFarland et al.* October 2002
90. **Ozone Effects on Net Primary Production and Carbon Sequestration in the U.S. Using a Biogeochemistry Model** *Felzer et al.* November 2002
91. **Exclusionary Manipulation of Carbon Permit Markets: A Laboratory Test** *Carlén* November 2002
92. **An Issue of Permanence: Assessing the Effectiveness of Temporary Carbon Storage** *Herzog et al.* December 2002
93. **Is International Emissions Trading Always Beneficial?** *Babiker et al.* December 2002
94. **Modeling Non-CO₂ Greenhouse Gas Abatement** *Hyman et al.* December 2002
95. **Uncertainty Analysis of Climate Change and Policy Response** *Webster et al.* December 2002
96. **Market Power in International Carbon Emissions Trading: A Laboratory Test** *Carlén* January 2003
97. **Emissions Trading to Reduce Greenhouse Gas Emissions in the United States: The McCain-Lieberman Proposal** *Paltsev et al.* June 2003
98. **Russia's Role in the Kyoto Protocol** *Bernard et al.* Jun '03
99. **Thermohaline Circulation Stability: A Box Model Study** *Lucarini & Stone* June 2003
100. **Absolute vs. Intensity-Based Emissions Caps** *Ellerman & Sue Wing* July 2003
101. **Technology Detail in a Multi-Sector CGE Model: Transport Under Climate Policy** *Schafer & Jacoby* July 2003
102. **Induced Technical Change and the Cost of Climate Policy** *Sue Wing* September 2003
103. **Past and Future Effects of Ozone on Net Primary Production and Carbon Sequestration Using a Global Biogeochemical Model** *Felzer et al.* (revised) January 2004
104. **A Modeling Analysis of Methane Exchanges Between Alaskan Ecosystems and the Atmosphere** *Zhuang et al.* November 2003

Contact the Joint Program Office to request a copy. The Report Series is distributed at no charge.

REPORT SERIES of the MIT Joint Program on the Science and Policy of Global Change

105. **Analysis of Strategies of Companies under Carbon Constraint** Hashimoto January 2004
106. **Climate Prediction: The Limits of Ocean Models** Stone February 2004
107. **Informing Climate Policy Given Incommensurable Benefits Estimates** Jacoby February 2004
108. **Methane Fluxes Between Terrestrial Ecosystems and the Atmosphere at High Latitudes During the Past Century** Zhuang et al. March 2004
109. **Sensitivity of Climate to Diapycnal Diffusivity in the Ocean** Dalan et al. May 2004
110. **Stabilization and Global Climate Policy** Sarofim et al. July 2004
111. **Technology and Technical Change in the MIT EPPA Model** Jacoby et al. July 2004
112. **The Cost of Kyoto Protocol Targets: The Case of Japan** Paltsev et al. July 2004
113. **Economic Benefits of Air Pollution Regulation in the USA: An Integrated Approach** Yang et al. (revised) Jan. 2005
114. **The Role of Non-CO₂ Greenhouse Gases in Climate Policy: Analysis Using the MIT IGSM** Reilly et al. Aug. '04
115. **Future U.S. Energy Security Concerns** Deutch Sep. '04
116. **Explaining Long-Run Changes in the Energy Intensity of the U.S. Economy** Sue Wing Sept. 2004
117. **Modeling the Transport Sector: The Role of Existing Fuel Taxes in Climate Policy** Paltsev et al. November 2004
118. **Effects of Air Pollution Control on Climate** Prinn et al. January 2005
119. **Does Model Sensitivity to Changes in CO₂ Provide a Measure of Sensitivity to the Forcing of Different Nature?** Sokolov March 2005
120. **What Should the Government Do To Encourage Technical Change in the Energy Sector?** Deutch May '05
121. **Climate Change Taxes and Energy Efficiency in Japan** Kasahara et al. May 2005
122. **A 3D Ocean-Seaice-Carbon Cycle Model and its Coupling to a 2D Atmospheric Model: Uses in Climate Change Studies** Dutkiewicz et al. (revised) November 2005
123. **Simulating the Spatial Distribution of Population and Emissions to 2100** Asadoorian May 2005
124. **MIT Integrated Global System Model (IGSM) Version 2: Model Description and Baseline Evaluation** Sokolov et al. July 2005
125. **The MIT Emissions Prediction and Policy Analysis (EPPA) Model: Version 4** Paltsev et al. August 2005
126. **Estimated PDFs of Climate System Properties Including Natural and Anthropogenic Forcings** Forest et al. September 2005
127. **An Analysis of the European Emission Trading Scheme** Reilly & Paltsev October 2005
128. **Evaluating the Use of Ocean Models of Different Complexity in Climate Change Studies** Sokolov et al. November 2005
129. **Future Carbon Regulations and Current Investments in Alternative Coal-Fired Power Plant Designs** Sekar et al. December 2005
130. **Absolute vs. Intensity Limits for CO₂ Emission Control: Performance Under Uncertainty** Sue Wing et al. January 2006
131. **The Economic Impacts of Climate Change: Evidence from Agricultural Profits and Random Fluctuations in Weather** Deschenes & Greenstone January 2006
132. **The Value of Emissions Trading** Webster et al. Feb. 2006
133. **Estimating Probability Distributions from Complex Models with Bifurcations: The Case of Ocean Circulation Collapse** Webster et al. March 2006
134. **Directed Technical Change and Climate Policy** Otto et al. April 2006
135. **Modeling Climate Feedbacks to Energy Demand: The Case of China** Asadoorian et al. June 2006
136. **Bringing Transportation into a Cap-and-Trade Regime** Ellerman, Jacoby & Zimmerman June 2006
137. **Unemployment Effects of Climate Policy** Babiker & Eckaus July 2006
138. **Energy Conservation in the United States: Understanding its Role in Climate Policy** Metcalf Aug. '06
139. **Directed Technical Change and the Adoption of CO₂ Abatement Technology: The Case of CO₂ Capture and Storage** Otto & Reilly August 2006
140. **The Allocation of European Union Allowances: Lessons, Unifying Themes and General Principles** Buchner et al. October 2006
141. **Over-Allocation or Abatement? A preliminary analysis of the EU ETS based on the 2006 emissions data** Ellerman & Buchner December 2006
142. **Federal Tax Policy Towards Energy** Metcalf Jan. 2007
143. **Technical Change, Investment and Energy Intensity** Kratena March 2007
144. **Heavier Crude, Changing Demand for Petroleum Fuels, Regional Climate Policy, and the Location of Upgrading Capacity** Reilly et al. April 2007
145. **Biomass Energy and Competition for Land** Reilly & Paltsev April 2007
146. **Assessment of U.S. Cap-and-Trade Proposals** Paltsev et al. April 2007
147. **A Global Land System Framework for Integrated Climate-Change Assessments** Schlosser et al. May 2007
148. **Relative Roles of Climate Sensitivity and Forcing in Defining the Ocean Circulation Response to Climate Change** Scott et al. May 2007
149. **Global Economic Effects of Changes in Crops, Pasture, and Forests due to Changing Climate, CO₂ and Ozone** Reilly et al. May 2007
150. **U.S. GHG Cap-and-Trade Proposals: Application of a Forward-Looking Computable General Equilibrium Model** Gurgel et al. June 2007
151. **Consequences of Considering Carbon/Nitrogen Interactions on the Feedbacks between Climate and the Terrestrial Carbon Cycle** Sokolov et al. June 2007
152. **Energy Scenarios for East Asia: 2005-2025** Paltsev & Reilly July 2007
153. **Climate Change, Mortality, and Adaptation: Evidence from Annual Fluctuations in Weather in the U.S.** Deschênes & Greenstone August 2007

Contact the Joint Program Office to request a copy. The Report Series is distributed at no charge.

REPORT SERIES of the MIT Joint Program on the Science and Policy of Global Change

- 154. Modeling the Prospects for Hydrogen Powered Transportation Through 2100** *Sandoval et al.* February 2008
- 155. Potential Land Use Implications of a Global Biofuels Industry** *Gurgel et al.* March 2008
- 156. Estimating the Economic Cost of Sea-Level Rise** *Sugiyama et al.* April 2008
- 157. Constraining Climate Model Parameters from Observed 20th Century Changes** *Forest et al.* April 2008
- 158. Analysis of the Coal Sector under Carbon Constraints** *McFarland et al.* April 2008
- 159. Impact of Sulfur and Carbonaceous Emissions from International Shipping on Aerosol Distributions and Direct Radiative Forcing** *Wang & Kim* April 2008
- 160. Analysis of U.S. Greenhouse Gas Tax Proposals** *Metcalf et al.* April 2008
- 161. A Forward Looking Version of the MIT Emissions Prediction and Policy Analysis (EPPA) Model** *Babiker et al.* May 2008
- 162. The European Carbon Market in Action: Lessons from the first trading period** Interim Report *Convery, Ellerman, & de Perthuis* June 2008
- 163. The Influence on Climate Change of Differing Scenarios for Future Development Analyzed Using the MIT Integrated Global System Model** *Prinn et al.* September 2008
- 164. Marginal Abatement Costs and Marginal Welfare Costs for Greenhouse Gas Emissions Reductions: Results from the EPPA Model** *Holak et al.* November 2008
- 165. Uncertainty in Greenhouse Emissions and Costs of Atmospheric Stabilization** *Webster et al.* November 2008
- 166. Sensitivity of Climate Change Projections to Uncertainties in the Estimates of Observed Changes in Deep-Ocean Heat Content** *Sokolov et al.* November 2008
- 167. Sharing the Burden of GHG Reductions** *Jacoby et al.* November 2008
- 168. Unintended Environmental Consequences of a Global Biofuels Program** *Melillo et al.* January 2009
- 169. Probabilistic Forecast for 21st Century Climate Based on Uncertainties in Emissions (without Policy) and Climate Parameters** *Sokolov et al.* January 2009
- 170. The EU's Emissions Trading Scheme: A Proto-type Global System?** *Ellerman* February 2009
- 171. Designing a U.S. Market for CO₂** *Parsons et al.* February 2009
- 172. Prospects for Plug-in Hybrid Electric Vehicles in the United States & Japan: A General Equilibrium Analysis** *Karplus et al.* April 2009
- 173. The Cost of Climate Policy in the United States** *Paltsev et al.* April 2009
- 174. A Semi-Empirical Representation of the Temporal Variation of Total Greenhouse Gas Levels Expressed as Equivalent Levels of Carbon Dioxide** *Huang et al.* June 2009
- 175. Potential Climatic Impacts and Reliability of Very Large Scale Wind Farms** *Wang & Prinn* June 2009
- 176. Biofuels, Climate Policy and the European Vehicle Fleet** *Gitaux et al.* August 2009
- 177. Global Health and Economic Impacts of Future Ozone Pollution** *Selin et al.* August 2009
- 178. Measuring Welfare Loss Caused by Air Pollution in Europe: A CGE Analysis** *Nam et al.* August 2009
- 179. Assessing Evapotranspiration Estimates from the Global Soil Wetness Project Phase 2 (GSWP-2) Simulations** *Schlosser and Gao* September 2009
- 180. Analysis of Climate Policy Targets under Uncertainty** *Webster et al.* September 2009
- 181. Development of a Fast and Detailed Model of Urban-Scale Chemical and Physical Processing** *Cohen & Prinn* October 2009
- 182. Distributional Impacts of a U.S. Greenhouse Gas Policy: A General Equilibrium Analysis of Carbon Pricing** *Rausch et al.* November 2009
- 183. Canada's Bitumen Industry Under CO₂ Constraints** *Chan et al.* January 2010
- 184. Will Border Carbon Adjustments Work?** *Winchester et al.* February 2010
- 185. Distributional Implications of Alternative U.S. Greenhouse Gas Control Measures** *Rausch et al.* June 2010
- 186. The Future of U.S. Natural Gas Production, Use, and Trade** *Paltsev et al.* June 2010
- 187. Combining a Renewable Portfolio Standard with a Cap-and-Trade Policy: A General Equilibrium Analysis** *Morris et al.* July 2010
- 188. On the Correlation between Forcing and Climate Sensitivity** *Sokolov* August 2010
- 189. Modeling the Global Water Resource System in an Integrated Assessment Modeling Framework: IGSM-WRS** *Strzepek et al.* September 2010
- 190. Climatology and Trends in the Forcing of the Stratospheric Zonal-Mean Flow** *Monier and Weare* January 2011
- 191. Climatology and Trends in the Forcing of the Stratospheric Ozone Transport** *Monier and Weare* January 2011
- 192. The Impact of Border Carbon Adjustments under Alternative Producer Responses** *Winchester* February 2011
- 193. What to Expect from Sectoral Trading: A U.S.-China Example** *Gavard et al.* February 2011
- 194. General Equilibrium, Electricity Generation Technologies and the Cost of Carbon Abatement** *Lanz and Rausch* February 2011
- 195. A Method for Calculating Reference Evapotranspiration on Daily Time Scales** *Farmer et al.* February 2011
- 196. Health Damages from Air Pollution in China** *Matus et al.* March 2011
- 197. The Prospects for Coal-to-Liquid Conversion: A General Equilibrium Analysis** *Chen et al.* May 2011

REPORT SERIES of the **MIT Joint Program on the Science and Policy of Global Change**

198. The Impact of Climate Policy on U.S. Aviation

Winchester et al. May 2011

199. Future Yield Growth: What Evidence from Historical

Data *Gitiaux et al.* May 2011

**200. A Strategy for a Global Observing System for
Verification of National Greenhouse Gas Emissions**

Prinn et al. June 2011

201. Russia's Natural Gas Export Potential up to 2050

Paltsev July 2011

**202. Distributional Impacts of Carbon Pricing: A General
Equilibrium Approach with Micro-Data for Households**

Rausch et al. July 2011

203. Global Aerosol Health Impacts: Quantifying

Uncertainties *Selin et al.* August 2011

**204. Implementation of a Cloud Radiative Adjustment
Method to Change the Climate Sensitivity of CAM3**

Sokolov and Monier September 2011

205. Quantifying the Likelihood of Regional Climate

Change: A Hybridized Approach *Schlosser et al.* Oct 2011